NEA NUCLEAR SCIENCE COMMITTEE
NEA COMMITTEE ON SAFETY OF NUCLEAR INSTALLATIONS

NUPEC BWR FULL-SIZE FINE-MESH BUNDLE TEST (BFBT) BENCHMARK

Volume I: Specifications

B. Neykov, F. Aydogan, L. Hochreiter, K. Ivanov
Nuclear Engineering Program
The Pennsylvania State University
University Park, PA 16802, USA

H. Utsuno, K. Fumio
Japan Nuclear Energy Safety Organization
Kamiya-cho MT Bldg., 4-3-20, Toranomon, Minato-ku,
Tokyo, 105-0001, Japan

E.Sartori
OECD Nuclear Energy Agency
12 boulevard des Iles
92130 Issy les Moulineaux, France

May 2005

US NRC

OECD Nuclear Energy Agency

ORGANISATION FOR ECONOMIC CO-OPERATION AND DEVELOPMENT

Pursuant to Article 1 of the Convention signed in Paris on 14th December 1960, and which came into force on 30th September 1961, the Organisation for Economic Co-operation and Development (OECD) shall promote policies designed:

- to achieve the highest sustainable economic growth and employment and a rising standard of living in Member countries, while maintaining financial stability, and thus to contribute to the development of the world economy;
- to contribute to sound economic expansion in Member as well as non-member countries in the process of economic development; and
- to contribute to the expansion of world trade on a multilateral, non-discriminatory basis in accordance with international obligations.

The original Member countries of the OECD are Austria, Belgium, Canada, Denmark, France, Germany, Greece, Iceland, Ireland, Italy, Luxembourg, the Netherlands, Norway, Portugal, Spain, Sweden, Switzerland, Turkey, the United Kingdom and the United States. The following countries became Members subsequently through accession at the dates indicated hereafter; Japan (28th April 1964), Finland (28th January 1969), Australia (7th June 1971), New Zealand (29th May 1973), Mexico (18th May 1994), the Czech Republic (21st December 1995), Hungary (7th May 1996), Poland (22nd November 1996) and the Republic of Korea (12th December 1996). The Commission of the European Communities takes part in the work of the OECD (Article 13 of the OECD Convention).

NUCLEAR ENERGY AGENCY

The OECD Nuclear Energy Agency (NEA) was established on 1st February 1958 under the name of OEEC European Nuclear Energy Agency. It received its present designation on 20th April 1972, when Japan became its first non-European full Member. NEA membership today consists of all OECD Member countries, except New Zealand and Poland. The Commission of the European Communities takes part in the work of the Agency.

The primary objective of the NEA is to promote co-operation among the governments of its participating countries in furthering the development of nuclear power as a safe, environmentally acceptable and economic energy source.

This is achieved by:

- *encouraging harmonization of national regulatory policies and practices, with particular reference to the safety of nuclear installations, protection of man against ionising radiation and preservation of the environment, radioactive waste management, and nuclear third party liability and insurance;*
- *assessing the contribution of nuclear power to the overall energy supply by keeping under review the technical and economic aspects of nuclear power growth and forecasting demand and supply for the different phases of the nuclear fuel cycle;*
- *developing exchanges of scientific and technical information particularly through participation in common services;*
- *setting up international research and development programmes and joint undertakings.*

In these and related tasks, the NEA works in close collaboration with the International Atomic Energy Agency in Vienna, with which it has concluded a Co-operation Agreement, as well as with other international organisations in the nuclear field.

Foreword

The need to refine models for best-estimate calculations, based on good-quality experimental data, has been expressed in many recent meetings in the field of nuclear applications. The needs arising in this respect should not be limited to the currently available macroscopic approaches but should be extended to next-generation approaches that focus on more microscopic processes. One most valuable database identified for the thermal-hydraulics modeling was developed by the Nuclear Power Engineering Corporation (NUPEC), Japan which includes sub-channel void fraction measurements in a representative BWR fuel assembly. Part of this database is made available for this international benchmark activity entitled as the NUPEC BWR Full-size Fine-Mesh Bundle Tests (BFBT) benchmark. This international project is officially approved by the Japan Ministry of Economy, Trade, and Industry (METI), US Nuclear Regulatory Commission (NRC), and endorsed by the OECD/NEA. The benchmark team is organized based on the collaboration between Japan and USA. A large number of international experts have agreed to contribute to this study.

The fine-mesh high-quality sub-channel void fraction and critical power data encourages advancement in the insufficiently developed field of the two-phase flow theory. Considering that the present theoretical approach is relatively immature, the benchmark specification is designed so that it will systematically assess and compare the participants' numerical models on the prediction of detailed void distributions and critical powers. The development of truly mechanistic models for critical power prediction is currently underway. These innovative models should include elementary processes such as void distributions, droplet deposition, liquid film entrainment, etc. The benchmark problem includes both macroscopic and microscopic measurement data. In this context, the sub-channel grade void fraction data are regarded as the macroscopic data and the digitized computer graphic images are the microscopic data.

The NUPEC BFBT benchmark consists of two parts (phases). Each part is consisting of different exercises:

- **Phase 1 – Void Distribution Benchmark**
  Exercise 1 – Steady-state sub-channel grade benchmark
  Exercise 2 – Steady-state microscopic grade benchmark
  Exercise 3 – Transient macroscopic grade benchmark

- **Phase 2 – Critical Power Benchmark**
  Exercise 1 –Steady-state benchmark
  Exercise 2 – Transient benchmark

This report provides the specifications for the international OECD/NRC NUPEC BFBT benchmark problem. The specification report is prepared jointly by the Pennsylvania State University (PSU), USA and Japan Nuclear Energy Safety (JNES) Organization, in cooperation with OECD/NEA,. The work is sponsored by the US NRC, METI-Japan, NEA/OECD, and the Nuclear Engineering Program (NEP), PSU. The specifications cover the three exercises of Phase 1, and the two exercises of Phase 2. In addition a CD-ROM has also been prepared with the complete NUPEC BWR database and is distributed along with the specifications to the participants, who have signed the NEA/OECD confidentiality agreement. The agreement as well as the other related information about the OECD/NRC BFBT benchmark can be found at:

http://www.nea.fr/html/science/egrsltb/BFBT/.

Acknowledgments

The authors would like to thank Prof. Hideki Nariai – President of the JNES, Japan, whose support and encouragement in establishing and carrying out this benchmark are invaluable.

This report is the sum of many efforts, the participants, the funding agencies and their staff – the METI, Japan, US NRC and the Organization of Economic Co-operation and Development (OECD). Special appreciation goes to the report reviewers: Maria N. Avramova and Andrew Ireland from Penn State University. Their comments and suggestions were very valuable and significantly improved the quality of this report.

The authors wish to express their sincere appreciation for the outstanding support offered by the JNES personnel in providing the test data and discussing the test characteristics.

Particularly noteworthy are the efforts of Farouk Eltawila and Gene Rhee from US NRC. With their help funding is secured, enabling this project to proceed. We also thank them for their excellent technical advice and assistance.

The authors would like to thank Dr. A. Hotta from TEPSYS, Japan, Prof. J. Aragones from Universidad Politecnica Madrid (UPM), Spain – member of NSC /NEA, and Prof. F. D'Auria of University of Pisa (UP), Italy – member of CSNI/NEA, whose support and encouragement in establishing and carrying out this benchmark are invaluable.

The authors wish to express their appreciation to Paul Clare for his help in improving the information on the grid a ferrule spacers.

Finally, we are grateful to Andrea Griffin-Chahid for having devoted her competence and skills to the final editing of this report.

TABLE OF CONTENTS

List of Figures

List of Tables

Chapter 1

INTRODUCTION

1.1 Background

In the past decade, a large amount of effort has been made toward the direct simulation of the boiling transition (BT) for boiling water reactor (BWR) fuel bundles. The most advanced sub-channel codes explicitly take into account entrained droplet behavior along with liquid film and vapor. Their calculations predict the dry-out process as disappearance of the liquid film on the fuel rod surface considering the competing mechanisms of entrainment, deposition and evaporation. Through a series of benchmark comparisons with full length/scale bundle data, it was verified that the codes are reliable in predicting the critical power of the conventional BWR fuel types. However, these sub-channel codes are not yet utilized in new fuel designs. Adequacy of fuel lattice geometries, spacer configurations, etc., is still confirmed mainly by costly experiments using partial- and full-scale mock-ups. The main reason for this situation is a shortage of high resolution and full-scale experimental data, on a sub-channel basis, under actual operating conditions.

The detailed void distribution inside the fuel bundle has been regarded as one of the important factors in the boiling transition in BWRs. With regard to the sub-channel void distribution, it is clear that the cross-flow through the sub-channel gap can dominate the void distribution in the sub-channel.

Most of the well-known sub-channel codes still employ the classical Lahey's void drift model [1] or modified versions of this model. Although there have been substantial efforts to establish a sound theoretical background of detailed void distributions, models that have been verified over a wide range of geometrical and thermal-hydraulic conditions are not yet available. In this sense, this subject still remains as a major unsolved problem for two-phase flow in BWR fuel bundles. The main reason for this lack of resolution is the lack of a reliable full bundle database under prototypical operating conditions. Up to now, only partial bundle (3×3 or 4×4) test data under relatively low pressure (≈ 1 MPa) conditions have been made available [2-3].

During the 4th OECD/NRC BWR TT Benchmark Workshop on 6 October 2002 in Seoul, Korea, the need to refine models for best-estimate calculations based on good-quality experimental data was discussed [4]. It was believed that the need arising in this respect should not be limited to currently available macroscopic approaches but should be extended to next-generation analysis and techniques that focus on a more microscopic process. It was suggested that a new international benchmark be established based on data made available from the NUPEC (Nuclear Power Engineering Corporation) database obtained in Japan. From 1987 to 1995, NUPEC performed a series of void measurement tests using full-size mock-up tests for both BWRs and pressurized water reactors (PWRs) [5]. Based on state-of-the-art computer tomography (CT) technology, the void distribution was visualized at the mesh size smaller than the sub-channel under actual plant conditions. NUPEC also performed steady-state and transient critical power test series based on the equivalent full-size mock-ups. Considering the reliability not only of the measured data, but also other relevant parameters such as the system pressure, inlet sub-cooling and rod surface temperature, these test series supplied the first substantial database for the development of truly mechanistic and consistent models for void distribution and boiling transition on a sub-channel basis.

1.2 Objective

The established international OECD/NRC BWR Full-Size Fine-Mesh Bundle Tests (BFBT) benchmark, based on the NUPEC database, encourages advancement in an uninvestigated field of two-phase flow, which has very important relevance to the nuclear reactor safety margin evaluation. Considering the immaturity of the theoretical approach, this benchmark specification is being designed so that it can systematically assess and compare the participants' numerical models for the prediction of detailed sub-channel void distributions and critical powers to full scale experimental data. Currently the numerical modeling of sub-channel void distribution has no theoretical approach that can be applied to a wide range of geometrical and operating conditions. In the past decade, experimental and computational technologies have tremendously improved the study of the two-phase flow structure. Over the next decade, it can be expected that mechanistic approaches will be more widely applied to the complicated two-phase fluid phenomena inside fuel bundles. The development of truly mechanistic models for critical power prediction is currently underway. These models must include elementary processes such as void distributions, droplet deposition, liquid film entrainment, and spacer grid behavior. The benchmark specification requires participants to explain their modeling correlations between the measured critical power and the two-phase flow dominant processes.

It should be recognized that the purpose of this benchmark is not only the comparison of currently available computational approaches but above-all the encouragement to develop novel next-generation approaches that focus on more microscopic processes. In this context, the sub-channel grade void fraction data are regarded as the macroscopic data and the digitized computer graphic images are the microscopic data. This benchmark specification is supplemented by a CD-ROM with complete NUPEC BWR Benchmark Database, which is distributed to all participants who have signed the confidentiality agreement.

1.3 Outline of the BFBT Specification

Chapter 1 discusses the main objectives of the international OECD/NRC BFBT benchmark. The definition of the benchmark phases and exercises is provided.

Chapter 2 of this report discusses the NUPEC BWR Full-size Fine-mesh Bundle Test (BFBT) Facility and the specific methods used in the void distribution and critical power measurements.

Chapter 3 provides the specifications of fuel assembly types and heater rods as well as the spacer data and thermo-mechanical properties of the structural materials.

Chapter 4 includes a description of the complete NUPEC BFBT database that is released by JNES, Japan. The complete benchmark database for all cases defined in the test matrixes is stored on CD-ROM, which is provided to the participants by NEA/OECD in addition to this specification.

Chapter 5 defines the NUPEC BFBT data to be used for the benchmark exercises. In total five exercises of two phases will be performed in the framework of this benchmark.

Chapter 6 describes the requested output and the output format that the benchmark team will collect from the participants.

1.4 Definition of Benchmark Phases

The test facility design and data from NUPEC includes both macroscopic and microscopic measurements. There are two separate phases, each of which consists of different exercises. These phases and exercises are discussed below.

1.4.1 Phase I - Void Distribution Benchmark

The purpose of this benchmark phase is three-fold:

1) To create numerical models of void distributions;
2) To create sound theoretical approach that could be employable to a wide range of geometrical and operating conditions;
3) To develop mechanistic approaches widely applicable to the two-phase fluid phenomena inside fuel bundles.

Phase I includes three exercises:

Exercise 1 – Steady-state sub-channel grade benchmark, where sub-channel, meso- and microscopic approaches can be used.

Exercise 2 – Steady-state microscopic grade benchmark, where meso- and microscopic approaches, and molecular dynamics can be utilized.

Exercise 3 – Transient macroscopic grade benchmark, where sub-channel approaches can be applied.

1.4.2 Phase II - Critical Power Benchmark

The purpose of this benchmark is to develop truly mechanistic models for critical power prediction.

Phase II includes two exercises:

Exercise 1 – Steady-state benchmark - applies one dimensional approach with BT correlations and sub-channel mechanistic approach.

Exercise 2 – Transient benchmark - applies one dimensional approach with BT correlations and sub-channel mechanistic approach.

1.5 Benchmark Team and Sponsorship

About thirty experts from twenty organizations in ten countries have confirmed their intention to participate. This international project is officially approved by METI, Japan, US NRC, and endorsed by the OECD/NEA. The benchmark team is organized based on the collaboration between Japan and the USA as shown in the Figure 1.5.1.

Figure 1.5.1 BFBT Benchmark Team

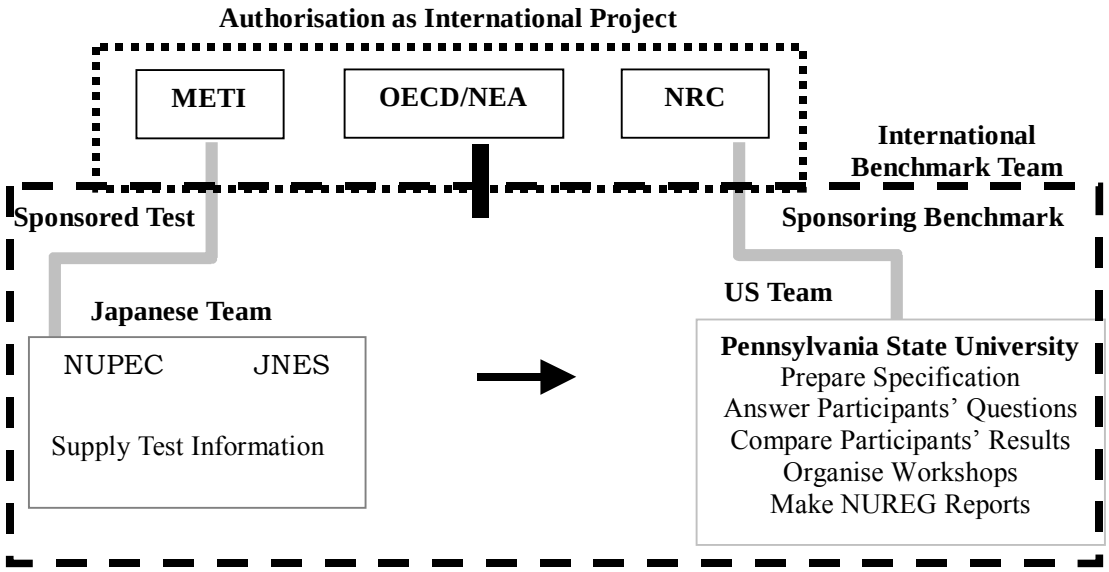

Chapter 2 TEST FACILITY

2.1 General

The void fraction distribution and critical power in a multi-rod assembly with a typical reactor power and fluid conditions has been measured in the NUPEC BWR Full-size Fine-mesh Bundle Test (BFBT) Facility. The facility is able to simulate the high-pressure, high temperature fluid conditions found in a BWR having an electrically-heated rod assembly that simulates a full scale BWR fuel assembly.

2.2 Test Loop

Figure 2.2.1 shows a diagram of the test loop. The main structural components are made of stainless steel (SUS304). De-mineralized water is used as a cooling fluid. The maximum operating conditions for the facility are 10.3 MPa in pressure, 315 °C in temperature, 12 MW in test power, and 75 t/h in flow rate. The test facility has a full range of steady-state testing capabilities over BWR operating conditions and can also simulate time-dependent characteristics of complicated BWR operational transients. Water is circulated by the circulation pump (1) and the coolant flow rate is controlled by the three valves (3) of different sizes. The inlet fluid temperature for the test section (5) is controlled by a direct-heating tubular pre-heater (4). Sub-cooled coolant flows upward into the test bundle (5), where it is heated and becomes a two-phase mixture. The steam is separated from the steam-water mixture in the separator (7) and is condensed using a spray of sub-cooled water in the steam drum (8). The condensed water is then returned to the circulation pump (1). The system pressure in both steady and transient state is controlled by spray lines (9), which have four different-sized valves. The pressurizer (6) controls the system pressure when the test assembly power is low. The spray pump (10) forces a spray into the steam-drum after water is cooled with two air-cooled heat exchangers (11). Based on this diagram, the test loop was operated covering the full range of BWR steady-state operating conditions.

2.3 Test section

The test section, shown in Figure 2.3.1, consists of a pressure vessel, a simulated flow channel, and electrodes. The full-scale BWR simulated fuel assembly was installed within the vessel. Two bundle types, the current 8×8 type and the high burn-up 8×8 type, were simulated. The dimensions for the different rod bundle arrays are summarized in Table 2.3.1. Chapter 3 of the BFBT specification provides detailed rod bundle geometry information. Each simulated rod in the test assembly is indirectly electrically heated to simulate a reactor fuel rod. The cladding, insulator, and heater were made of inconel, boron nitride, and nichrome, respectively.

Figure 2.3.1 System Diagram of Test Facility for NUPEC Rod Bundle Test Series

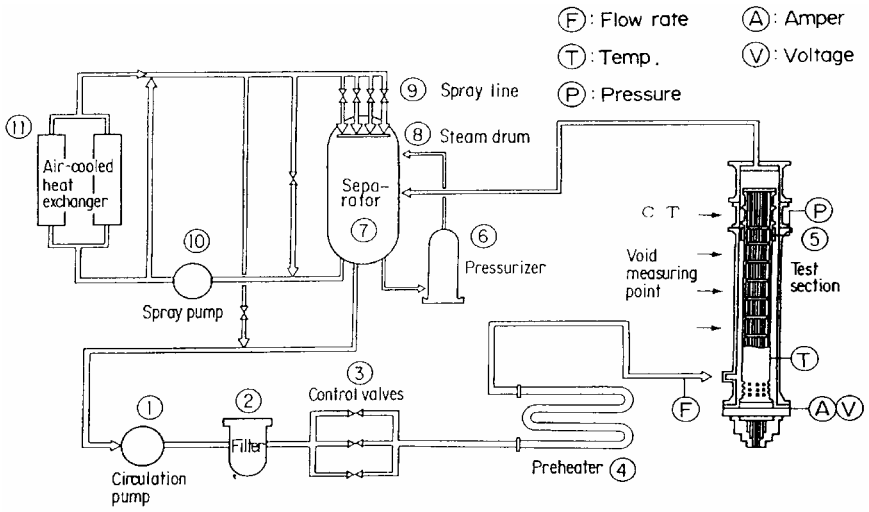

Figure 2.3.2 Cross-sectional View of Test Section

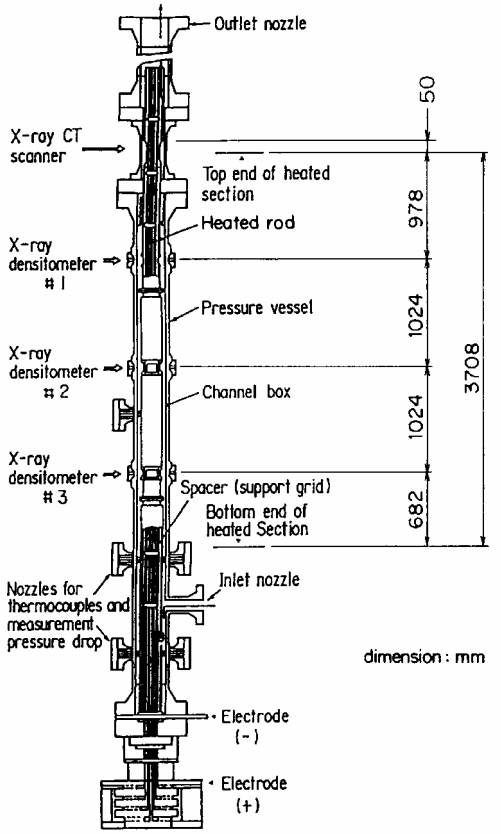

Table 2.3.1 Dimensions of BWR Test Bundles

Items	Current 8×8	High burnup 8×8
Number of fuel rods	62	60
Outer diameter (mm)	12.3	12.3
Heated length (m)	3.7	3.7
Number of water rod (mm)	2	1
Outer diameter of water rod (mm)	15.0	34.0
Rod pitch (mm)	16.2	16.2
Width of channel box	132.5	132.5
Number of spacer	7	7
Spacer type	Grid	Ferrule

2.4 Void Distribution Measurement Methods

Two types of void distribution measurement systems were employed as shown in Figure 2.4.1 (a), the X-ray CT scanner and the X-ray densitometer.

Fine mesh void distributions were measured using the X-ray CT scanner at a point 50 mm above the heated length under steady-state conditions. The measurement system and locations are shown in Figure 2.4.1 (b) and it consists of an X-ray tube and 512 detectors. Figure 2.4.1 (c) shows the void fraction measuring section, where the pressure vessel was made of titanium (Ti). The channel wall and the cladding of the heater rods at this location are made of beryllium (Be) to minimize X-ray attenuation in the structure. In order to avoid the effect of the two-phase flow fluctuations, the collection of projection data was repeated and the results were time-averaged. The attained spatial resolution was as small as 0.3 mm × 0.3 mm.

The cross-sectional average transient void distributions were measured by a X-ray densitometer. The measurement was performed at several middle elevations where the channel sections were made of beryllium (Be) and the heater rods had beryllium cladding of the same diameter as the Inconel portion of the heater rod.

Table 2.4.1 shows the basic specifications of the X-ray CT scanner. The X-ray beam is scanned over an object. An outline of the CT scanner principle is shown in Figure 2.4.1 (b). As it scans, a fan-shaped X-ray beam is attenuated by the object and the attenuated beam is measured by the detectors. The X-ray intensity data recorded by the detectors is called the projection data. The complete 360^{o} projection data are obtained for the object.

Figure 2.4.1 Void fraction measurement system

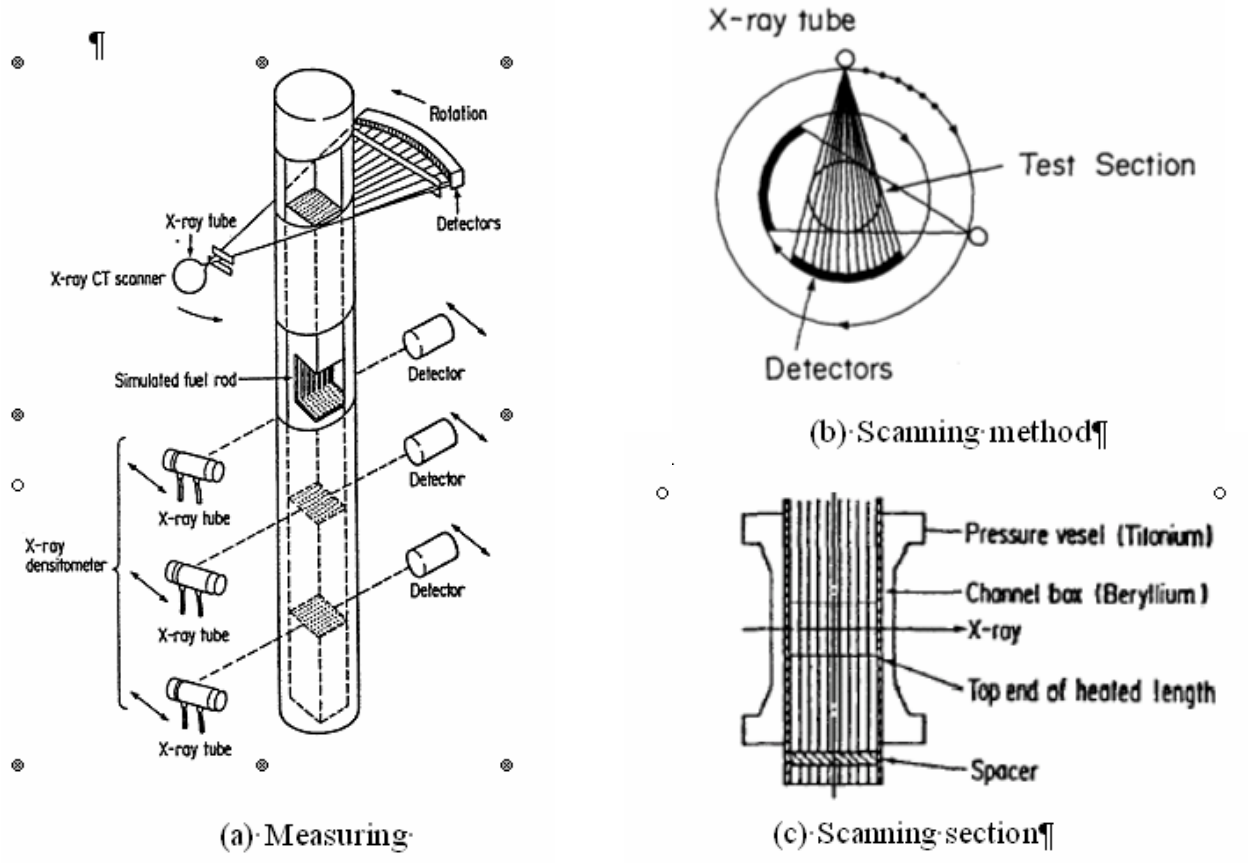

Table 2.4.1 Specification of X-ray CT Scanner

Scan method	**360° rotation with pulse X-rays**
Type of X-ray beam	Fan-shaped X-ray beam of 34° radiation angle
Voltage of X-ray tube	Max. 120 kV
Current	Max 400mA
Scanning time	15s
Scanning region	D=300 mm
Dimensions of reconstruction element	0.3mm X 0.3mm

The distribution of the linear attenuation coefficient is obtained by reconstructing the projection data. The reconstruction technique is called a filter back projection, and has been widely used in the field of nuclear medicine.

All void fraction signals from the detectors are calibrated using a signal from a reference detector to improve the signal-to-noise ratio.

Before performing actual void fraction measurements, position coordinates are calibrated at room temperature with the test section empty. They are then repeated with the section filled with water and at operating temperature with non-boiling water. Frequent measurements through a standard absorber are made to correct any electronic drift.

Absolute and differential pressures were measured using diaphragm transducers. The inlet flow rate was measured using turbine flow meter. The inlet sub-cooling was measured using double thermistors. In the heater rods, the surface temperature was monitored at positions just upstream of the spacers by the 0.5 mm diameter chromel-alumel thermocouples, which were located in the heater rod cladding

Table 2.4.2 shows the estimated accuracy of the various measurements. Three types of void fraction measurements were used: the local void fraction on a 0.3 mm × 0.3 mm square pixel element; the sub-channel-averaged void fraction, which is averaged over more than 400 pixel elements; and the cross–sectional averaged void fraction, which is averaged over more than 10^5 pixel elements. The accuracy of these void fraction measurements depends on the photon statistics of the X-ray source, the detector non-linearity, and the accuracy of the known fluid condition (temperature and pressure) measurements.

Table 2.4.2 Estimated Accuracy of Main process Parameters for Void Distribution Measurements

Quantity	Accuracy
Pressure	1%
Flow	1%
Power	1.5%
Inlet fluid temperature	1.5 Celsius
X-ray CT scanner	
Local void fraction	8%
Sub-channel void fraction	3%
Cross-sectional void fraction	2%
Spatial resolution	0.3 mm × 0.3 mm
Scanning time	15 seconds
X-ray densitometer	
Sampling time	Max. 60 seconds

Five different types of bundle assembly designs with different combinations of geometries and power shapes were tested in the void distribution experiments. BWR steady state and transient conditions were also simulated. Detailed information on the bundle assembly design and run conditions are presented in Chapters 3 and 4 of this report.

The steady state test series were performed using thermal-hydraulic conditions that envelope BWR bundle geometrical, power shape and two-phase flow parameters of actual plant steady-state operation. Both the X-ray CT scanner and the X-ray densitometer technique were used in the experiments. The range of test conditions was as follows: pressure - 1 - 8.6 MPa; flow rate - 284 - 1988 kg/m^2-s; and exit quality – 1 - 25%. In all, 476 measurement points were included.

Transient tests were performed to measure the cross-sectional averaged transient void fraction behavior over a range of pressure, flow, and power changes. The X-ray densitometer was used for this test. The following four operational transients were simulated since each one of them had a specific void variation: turbine trip without bypass; one pump trip; re-circulation pump tripped; and malfunction of pressure control system (pressure increase). The above four events include the combined effects of pressure, flow, and power with the resulting change in the bundle void distribution. In order to obtain the individual sensitivity of these process parameters, additional tests were performed in which only one of these three parameters was changed, at a time.

2.5 Critical Power Measurement Methods

The same test loop that was used in the void distribution measurements (Figure. 2.2.1) was also used for critical power measurements. The test loop was operated under normal BWR operational conditions and typical transient conditions corresponding to a one pump trip event and the turbine trip event.

The full scale test bundle, simulating the 8x8 high burn-up fuel, was installed in the test section. Three combinations of radial and axial power shapes were tested: 1) beginning of cycle (BOC) radial power pattern/cosine axial power shape (the C2A pattern); 2) end of cycle (EOC) radial power pattern/cosine axial power shape (C2B pattern); and 3) beginning of cycle radial power pattern/inlet peaked axial power shape (C3 pattern). The individual radial and axial power distributions for all three combinations are given in Chapter 3 of this report.

The steady-state test series consisted of two parts: pressure drop measurements and critical power tests. The pressure drop was measured in both single-phase flow and two-phase flow conditions that cover the normal operational behavior. The range of each test condition is given in Chapter 4. In total, 151 measurement points were run during the critical power test.

The critical power was measured by slowly increasing the bundle power while monitoring the individual heater rod thermocouple signals. The critical power was defined when the peak rod surface temperature became 14^{o}C higher than the steady-state temperature level before dry-out occurred. The dry-out was observed in the peak power rod located at the peripheral row adjacent to the channel box. The boiling transition was always observed just upstream of the spacer. The estimated accuracies of the major process parameters were equivalent to those in the void measurement tests listed in Table 2.4.2.

The bundle pressure drop was monitored at several locations as depicted in Figure 2.5.1

Figure 2.5.2 describes the definition of thermocouple position. Each thermocouple position is identified as follows: **Rod No. – Axial location – Rotational angle.** For example **16 – B – 270**

The rod surface temperature was also monitored at several locations as depicted in Figures 2.5.3 to 2.5.5.

Figure 2.5.1 Location of Pressure Taps for Critical Power Measurement

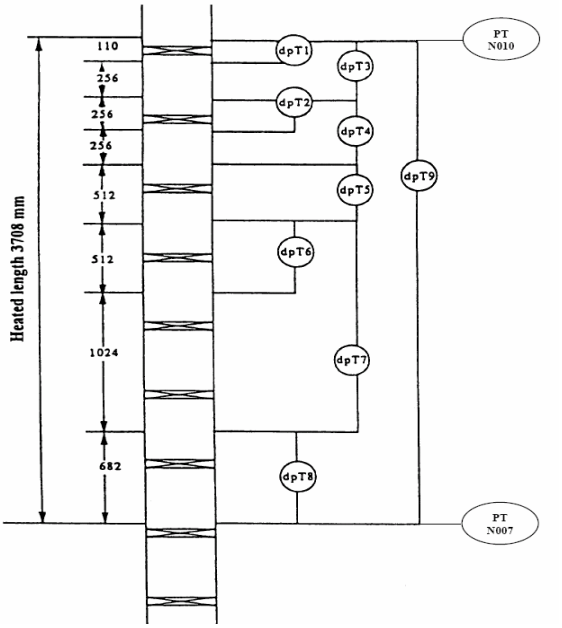

Figure 2.5.2 Definition of Thermocouple Position

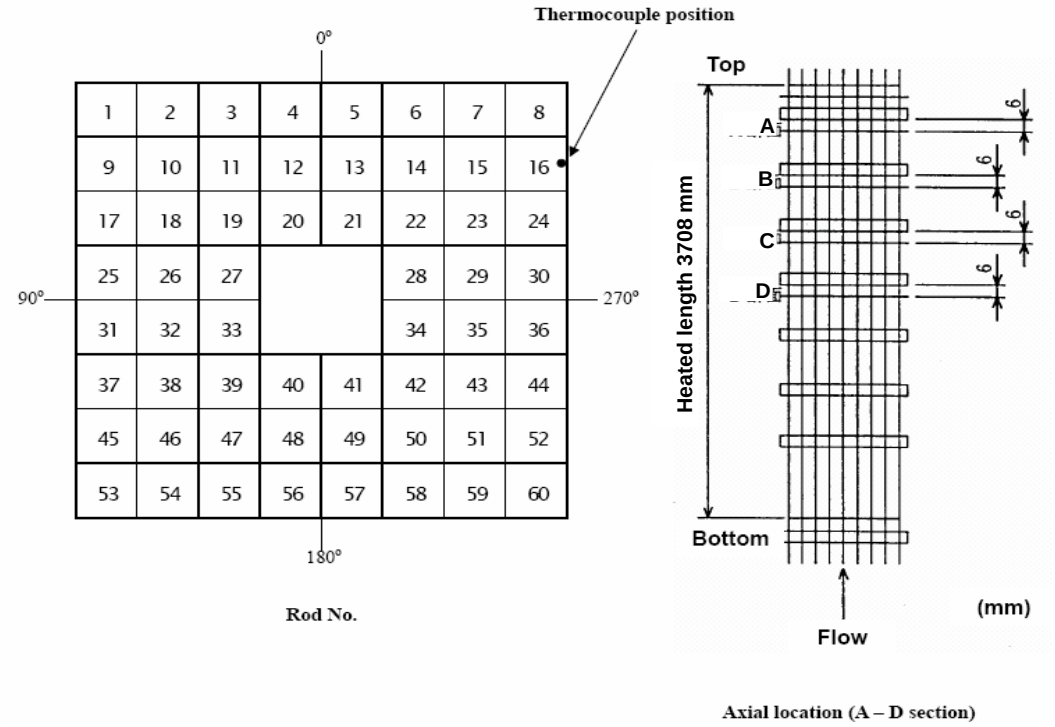

Figure 2.5.3 Location of Thermocouples for Critical Power Measurement (C2A)

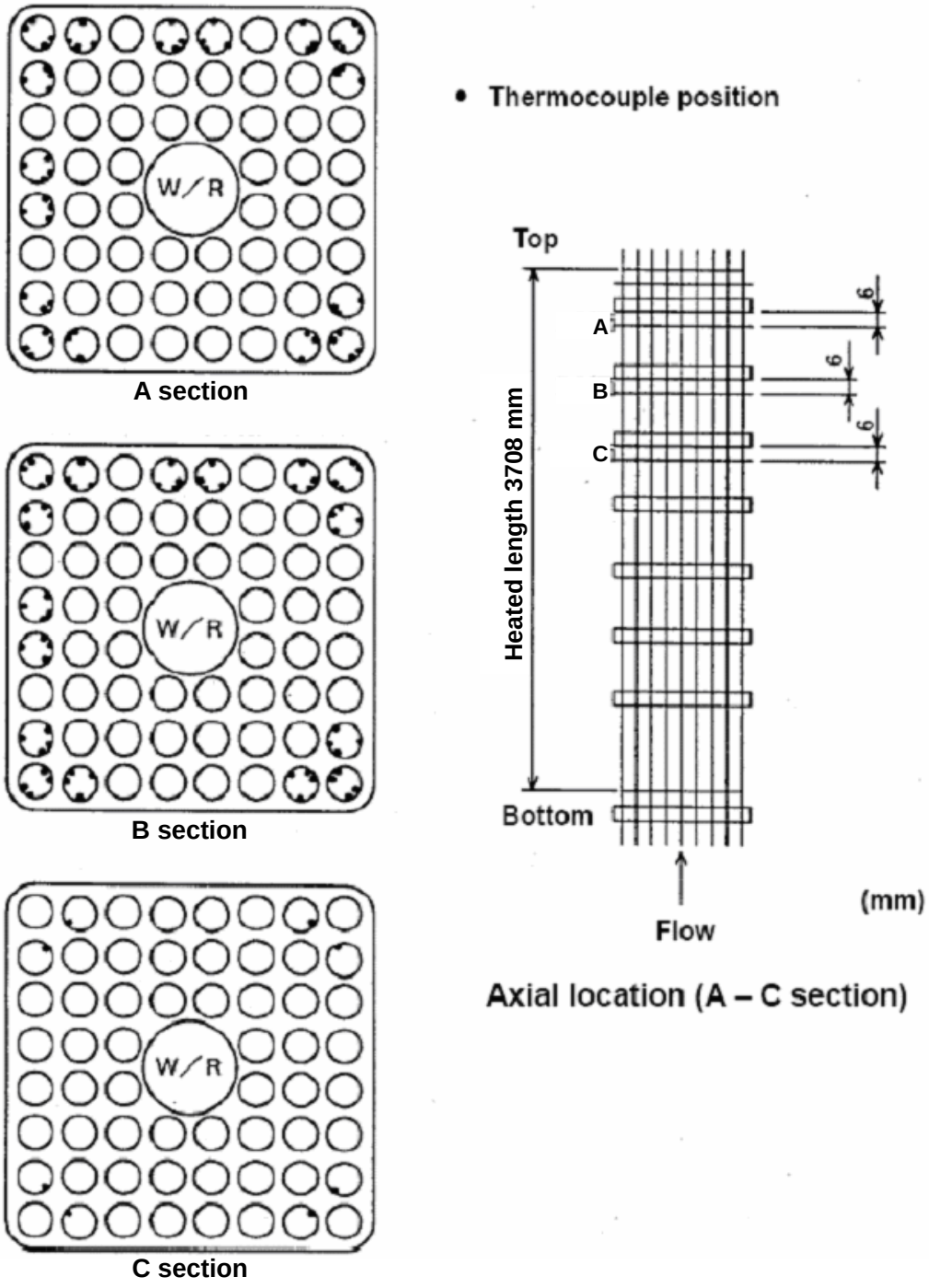

Figure 2.5.4 Location of Thermocouples for Critical Power Measurement (C2B)

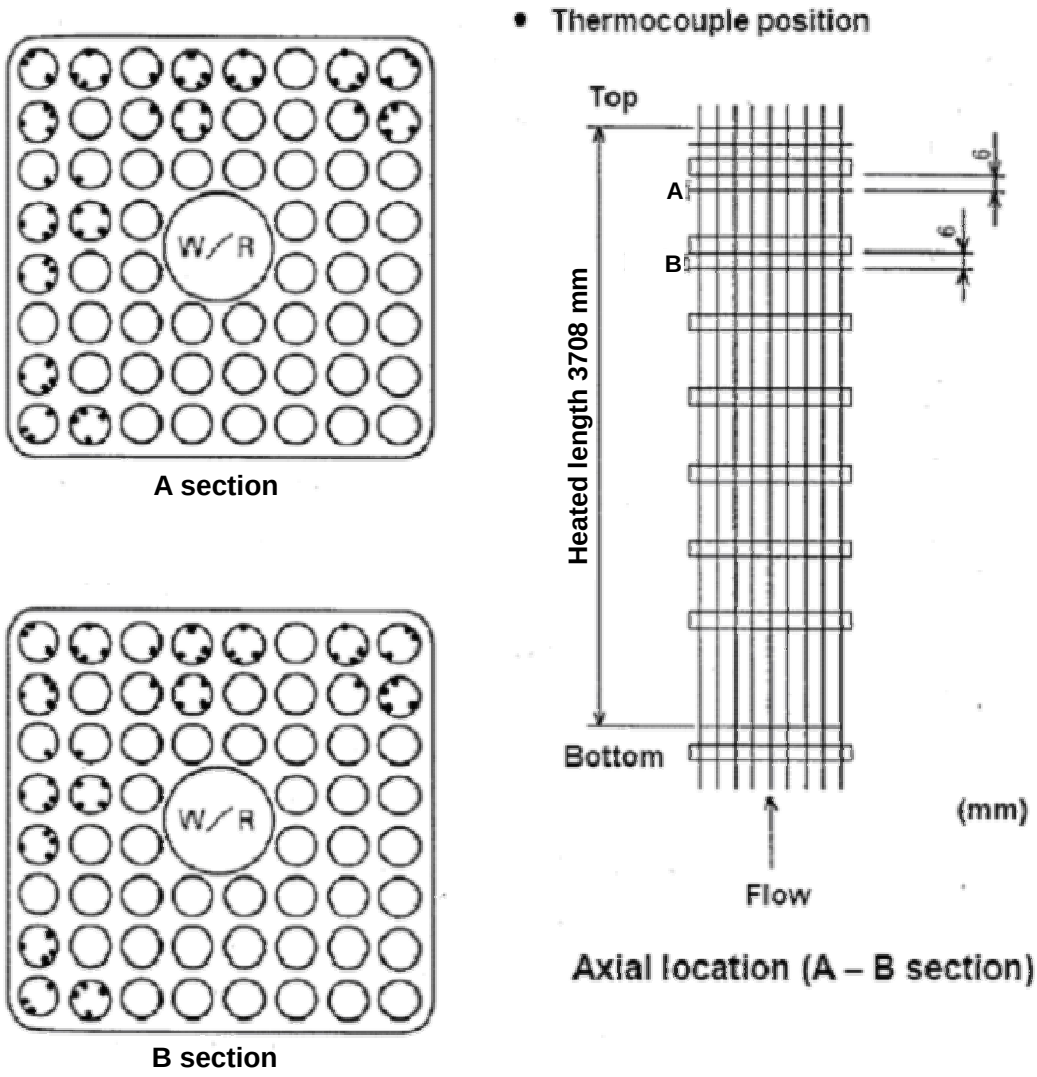

Figure 2.5.5 Location of Thermocouples for Critical Power Measurement (C3)

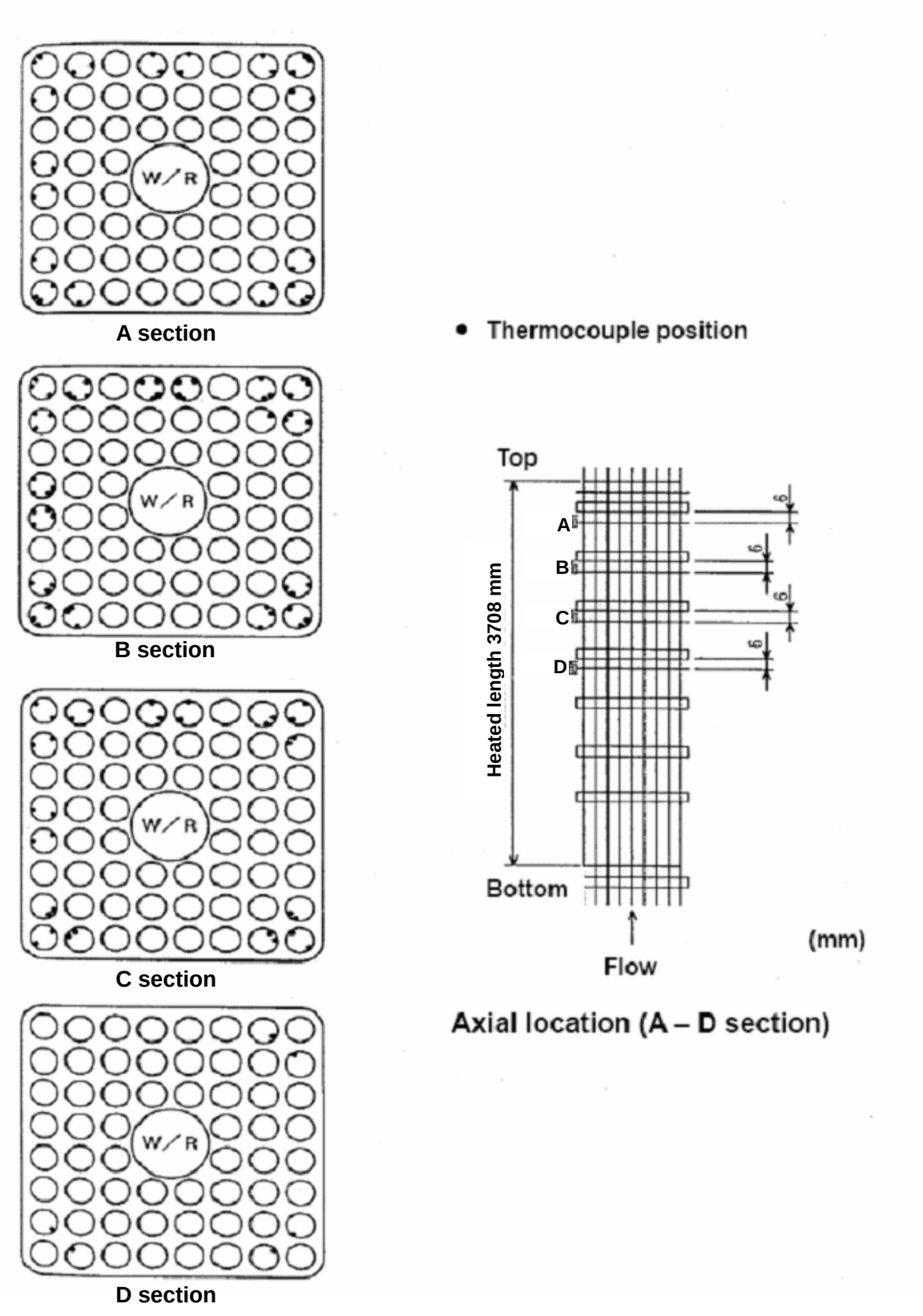

The transient test series simulated two typical BWR operational transients: 1) power transient: turbine trip event; and 2) flow transient: one recirculation pump trip event. The transient tests were separated in three types: license base transient tests; extreme scenario transient test; and post-boiling transition test. The objective of the license base transient test series was confirmation that the boiling transition never occurs during these transients. In the extreme scenario transient test, the initial power levels were increased to observe the boiling transition. The rod surface temperature was monitored. In the post-boiling transition test, the rod surface temperature was measured under the quasi-steady-state condition beyond the boiling transition. The main purpose of this test series was quantification of the post-dryout heat transfer coefficient.

The complete set of test conditions data for void distribution and critical power measurements are provided in Chapter 4 of this report.

Chapter 3

FUEL ASSEMBLY DATA

3.1 General

This chapter provides the participants with geometry and material data for the simulated BWR assemblies, spacers, and heated rods, which were utilized in the void distribution and critical power measurements. The power distribution patterns, radial and axial, as well as the tests conditions are described. Data for the fuel assemblies and spacers' dimensions, heater rods specifications, and material properties are also given.

3.2 Assembly Geometry Data

Two types of BWR assemblies are simulated in full length test facility, the current 8×8 fuel bundle and 8×8 high burn-up bundle. The dimensions of both bundles are given in Chapter 2, Table 2.3.1. In total, five different types of test assembly configurations with different combinations of bundle geometry and power profiles were used in the void distribution and critical power measurements.

Table.3.2.1 summarizes the five types (Type 0 to Type 4) of test assemblies used in the void distribution measurements.

Table 3.2.1 Test Assembly and Radial Power Distribution for Void Distribution Measurements

Test assembly No.	0	1	2	3	4
Fuel Type	Current use 8x8 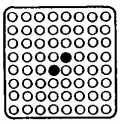				High burnup 8x8 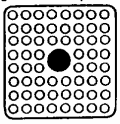
Planar power profile	Uniform	Simulated design profile	Simulated design profile	Simulated design profile	Simulated design profile
Axial power profile	Uniform	Cosine	Half-cosine	Inlet peak	Uniform
Heated length	Full	Full	Half	Full	Full
Axial powe distribution Axial → Power	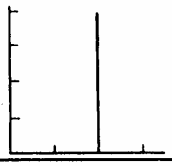	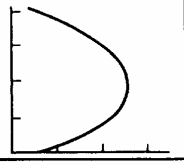	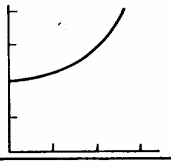	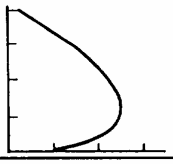	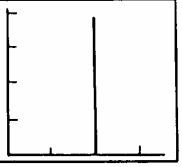

The test assembly No. 0 (as given in Table 3.2.1) has uniform radial power distribution. Using test bundle 0, three sub-type test assemblies No. 0 – No. 0-1; 0-2; and 0-3 – were used to examine the effects of radial power distribution on the void fraction distribution. The number of unheated rods was varied among these test assemblies. The radial arrangements of heated and unheated rods are shown in Figure 3.2.1. Test assembly No. 0-1 simulates a current BWR fuel assembly and has two unheated rods. Test assemblies No. 0-2 and No. 0-3 have four and nine unheated rods, respectively. Two water channels (rods) are present in all of these three sub-type test assemblies and they are counted as unheated rods. The radial power distribution for the heated rods is uniform and the axial power distribution is also uniform as shown in Table 3.2.1

Figure 3.2.1 Unheated Rods Arrangements in Test Assembly No. 0

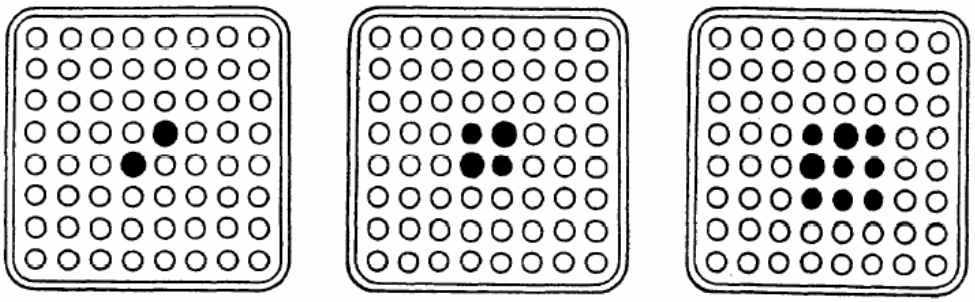

(a) 0-1 (b) 0-2 (c) 0-3

○ : Heated rod, ● : Unheated rod

Test assembly types 1, 2, 3, are like assembly type No. 0-1 with two unheated rods, but with different axial heated length – 3708 mm, 1747 mm and 3708 mm respectively and different axial power shapes. These assembly types have a design-simulated radial power profile as shown in Figure 3.2.2.

Table 3.2.2 Radial Power Shape of Test Assembly Types 1 ÷ 3

1.15	1.30	1.15	1.30	1.30	1.15	1.30	1.15
1.30	0.45	0.89	0.89	0.89	0.45	1.15	1.30
1.15	0.89	0.89	0.89	0.89	0.89	0.45	1.15
1.30	0.89	0.89	0.89		0.89	0.89	1.15
1.30	0.89	0.89		0.89	0.89	0.89	1.15
1.15	0.45	0.89	0.89	0.89	0.89	0.45	1.15
1.30	1.15	0.45	0.89	0.89	0.45	1.15	1.30
1.15	1.30	1.15	1.15	1.15	1.15	1.30	1.15

The tabulated data for all the three non-uniform axial power shapes, shown in Table 3.2.1, are given in Table 3.2.3. Only the full length tests will be examined as part of the Benchmark exercises.

Table 3.2.3 Axial Power Shape

Node	Relative power		
	Cosine – Test Assembly 1	**Half-cosine – Test Assembly 2**	**Inlet-peak – Test Assembly 3**
(Bottom)			0.53
1	0.46	0	0.83
2	0.58	0	1.00
3	0.69	0	1.17
4	0.79	0	1.28
5	0.88	0	1.34
6	0.99	0	1.37
7	1.09	0	1.39
8	1.22	0	1.40
9	1.22	0	1.39
10	1.34	0	1.37
11	1.34	0	1.34
12	1.40	0	1.28
13	1.40	0.46	1.21
14	1.34	0.58	1.10
15	1.34	0.69	1.00
16	1.22	0.79	0.89
17	1.22	0.88	0.79
18	1.09	0.99	0.71
19	0.99	1.09	0.64
20	0.88	1.22	0.58
21	0.79	1.22	0.53
22	0.69	1.34	0.46
23	0.58	1.34	0.40
24	0.46	1.40	
(Top)			

The axial power distributions given in Table 3.2.3 are also shown in Figure 3.2.2 a) for the cosine shape and Figure 3.2.2 b) for the inlet peak shape. The length between each step is 154.5 mm and there are 24 steps for the cosine shape, and 24 steps for the inlet peak shape. The constant power factor for each step is given in Figures 3.2.2 a) and 3.2.2 b), as well as Table 3.2.3.

Table 3.2.4 gives the three combinations of high burnup assemblies with different radial and axial power shapes, namely C2A, C2B and C3, which were utilized in the critical power measurements. Assemblies C2A and C3 simulate the high radial peaking condition at the beginning of operation while the assembly C2B simulates the high bundle power condition at the end of operation.

The radial power profiles for the beginning of operation (type A) and for the end of operation (type B) are given in Table 3.2.5. The axial power shapes, cosine and inlet-peaked, are shown in Figure 3.2.2 (values are the same as in Table 3.2.3).

Table 3.2.4 Test Assemblies and Radial Power Distributions for Critical Power Measurements

Test item	Critical power test		
Test assembly	C2A	C2B	C3
Fuel type	High burn-up 8 × 8		
Axial power shape	Cosine	Cosine	Inlet peak
Radial power shape	A	B	A

A – Simulation pattern for beginning of operation.
B – Simulation pattern for middle of operation.

Table 3.2.5 Radial Power Shape of Test Assembly Type 4

A (for Assembly 4, C2A, C3)

1.15	1.30	1.15	1.30	1.30	1.15	1.30	1.15
1.30	0.45	0.89	0.89	0.89	0.45	1.15	1.30
1.15	0.89	0.89	0.89	0.89	0.89	0.45	1.15
1.30	0.89	0.89			0.89	0.89	1.15
1.30	0.89	0.89			0.89	0.89	1.15
1.15	0.45	0.89	0.89	0.89	0.89	0.45	1.15
1.30	1.15	0.45	0.89	0.89	0.45	1.15	1.30
1.15	1.30	1.15	1.15	1.15	1.15	1.30	1.15

B (for Assembly C2B)

0.99	1.18	0.99	1.18	1.18	0.99	1.18	0.99
1.18	0.75	0.99	1.18	0.99	0.75	0.99	1.18
0.99	0.99	0.99	0.99	0.99	0.99	0.45	0.99
1.18	1.18	0.99			0.99	0.99	0.99
1.18	0.99	0.99			0.99	0.99	0.99
0.99	0.75	0.99	0.99	0.99	0.99	0.75	0.99
1.18	0.99	0.75	0.99	0.99	0.75	0.99	0.99
0.99	1.18	0.99	0.99	0.99	0.99	0.99	0.99

Figure 3.2.2 Axial Power Distribution Patterns for Critical Power Measurements

(a) Cosine shape

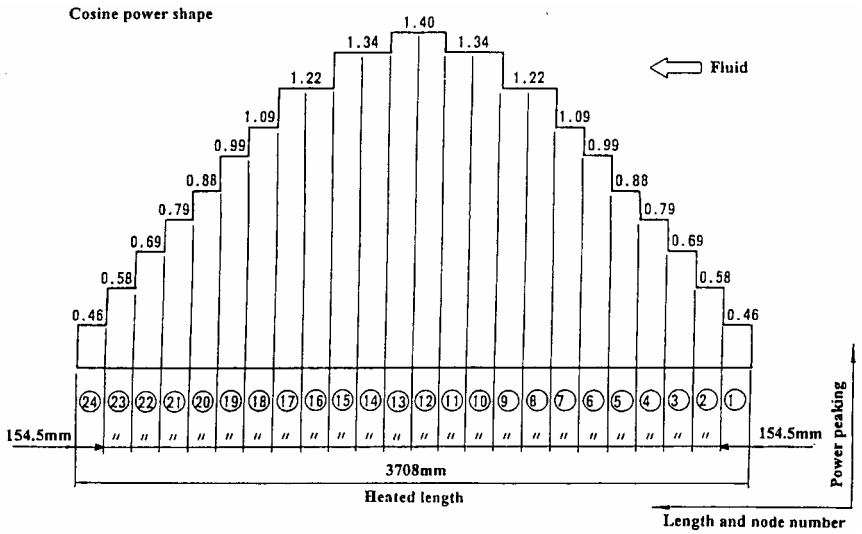

(b) Inlet peak shape

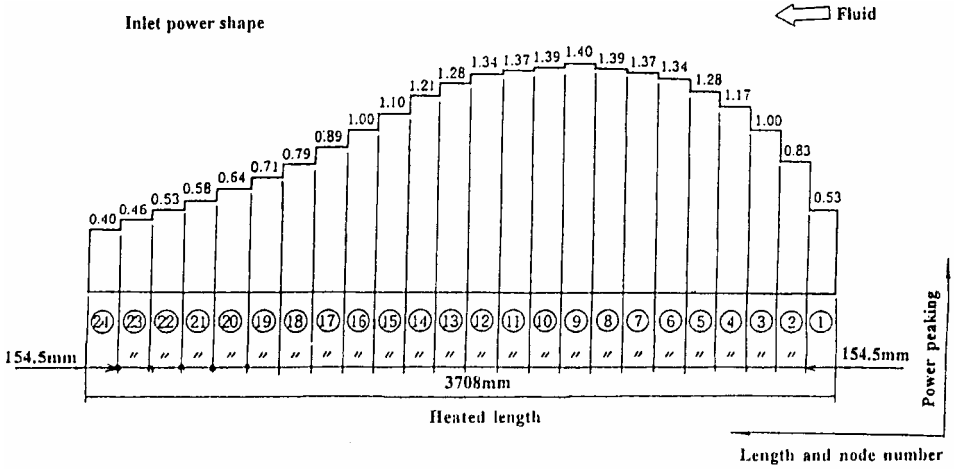

Both the reference test bundle - test assembly 0; and the high burn-up test bundle - test assembly 4, have a uniform axial power distribution as indicated in Table 3.2.1.

Table 3.2.6 provides the bundle geometry data for test bundles 0-1, 0-2 and 0-3. As this table indicates, the bundle axial and radial power distributions are uniform.

Table 3.2.6 Geometry and Power Shape of Test Assembly Types 0-1, 0-2 and 0-3

Item	Data		
Assembly	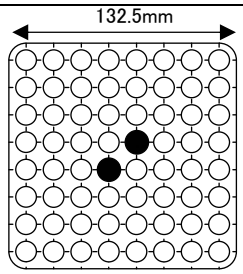	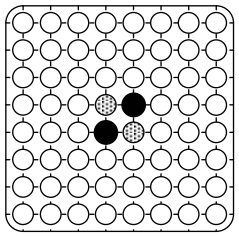	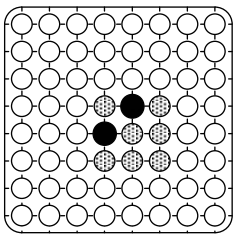
	0-1	0-2	0-3
Simulated fuel assembly type	8×8		
Number of heated rods	62	60	55
Number of unheated rods	0	2	7
Heated rods outer diameter (mm)	12.3		
Heated rods pitch (mm)	16.2		
Axial heated length (mm)	3708		
Number of water rods	2		
Water rods outer diameter (mm)	15.0		
Channel box inner width (mm)	132.5		
Channel box corner radius (mm)	8.0		
In channel flow area (mm^2)	9781		
Spacer type	Grid		
Number of spacers	7		
Spacer pressure loss coefficients	1.2		
Spacer location (mm)	455, 967, 1479, 1991, 2503, 3015, 3527 (Distance from bottom of heated length to spacer bottom face)		
Radial power shape	Uniform		
Axial power shape	Uniform		

○ : Heated rod ◍: Unheated rod ●: Water rod: no flow in water rods

Table 3.2.7 provides the geometry and power shape information for bundles 1, 2 and 3 from Table 3.2.1. There are different axial power distributions as given in Table 3.2.3 and Figures 3.2.2 a) and b). All the bundle designs use a spacer grid design, which will be discussed in section 3.4.

Table 3.2.7 Geometry and Power Shape of Test Assembly Types 1, 2 and 3

Item	Data		
Assembly	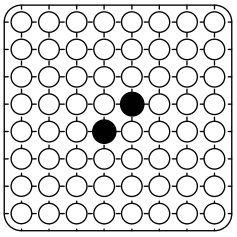	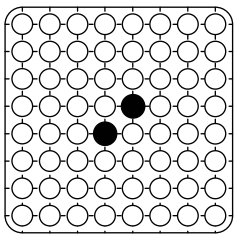	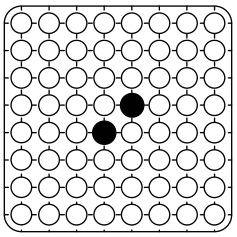
	1	2	3
Simulated fuel assembly type	8×8		
Number of heated rods	62		
Heated rods outer diameter (mm)	12.3		
Heated rods pitch (mm)	16.2		
Axial heated length (mm)	3708	1747	3708
Number of water rods	2		
Water rods outer diameter (mm)	15.0		
Channel box inner width (mm)	132.5		
Channel box corner radius (mm)	8.0		
In channel flow area (mm^2)	9781		
Spacer type	Grid		
Number of spacers	7		
Spacer pressure loss coefficients	1.2		
Spacer location (mm)	455, 967, 1479, 1991, 2503, 3015, 3527 (Distance from bottom of heated length to spacer bottom face)		
Radial power shape	Simulation pattern for beginning of operation		
Axial power shape	Cosine	Half-cosine	Inlet Peak

○ : Heated rod ◍: Unheated rod ●: Water rod: no flow in water rods

Assembly configuration 4 shown in Table 3.2.1 is designed as a high burn-up 8x8 fuel bundle, and has a large water rod at the center of the bundle. Table 3.2.8 gives the geometric information for the high burn-up bundle design. There were a total of four (4) different configurations tested for the high burn-up design as indicated in Table 3.2.8. The spacer grid used in these tests was a ferrule grid design, and it is discussed in Section 3.4.

Table 3.2.8 Geometry and Power Shape of Test Assembly Types 4, C2A, C2B and C3

Item	Data			
Test assembly	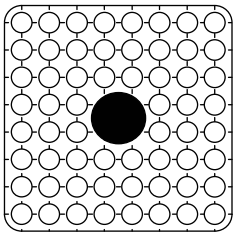			
	4	C2A	C2B	C3
Simulated fuel assembly type	High burn-up 8×8			
Number of heated rods	60			
Heated rods outer diameter (mm)	12.3			
Heated rods pitch (mm)	16.2			
Axial heated length (mm)	3708			
Number of water rods	1			
Water rods outer diameter (mm)	34.0			
Channel box inner width (mm)	132.5			
Channel box corner radius (mm)	8.0			
In channel flow area (mm^2)	9463			
Spacer type	Ferrule			
Number of spacers	7			
Spacer pressure loss coefficients	1.2			
Spacer location (mm)	455, 967, 1479, 1991, 2503, 3015, 3527 (Distance from bottom of heated length to spacer bottom face)			
Radial power shape	A	A	B	A
Axial power shape	Uniform	Cosine	Cosine	Inlet-peak

○ : Heated rod ●: Water rod: no flow in water rods
A: Simulation pattern for beginning of operation
B: Simulation pattern for middle of operation

3.3 Heater Rod Specification

Figure 3.3.1 shows the cross-sectional view of the heated rod. The rod is single-ended, grounded electrical heater rod, which represents the nuclear fuel rod. The heater rod structure is given in Table 3.3.1. The cladding insulator and heater are made of inconel, boron nitride and nichrome, respectively. The heated rod surface temperature is measured by 0.5 mm-diameter chromel-alumel thermocouples. Individual cladding thermocouples are embedded in the cladding surface. Axially, they are positioned mainly at positions just upstream of the spacers. Each heated rod is joined to an X-ray transmission section, which is of the same diameter as the heated rod but the cladding is made of beryllium (Be) for case of X-ray transmission.

Table 3.3.1 Heater rod structure

Item		Data
Heater	Outer diameter (mm)	7.3
	Material	Nichrome
Insulator	Outer diameter (mm)	9.7
	Material	Boron Nitride
Cladding	Thickness (mm)	1.3
	Material	Inconel 600/Berylium

Figure 3.3.1 Cross sectional view of heater rod

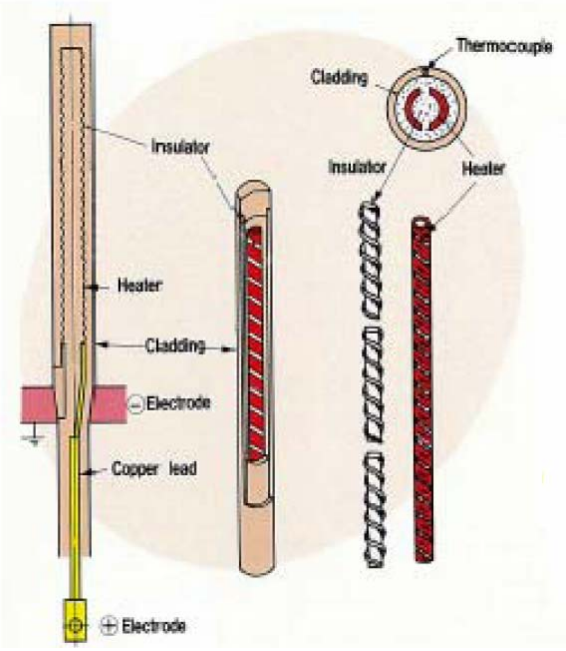

3.4 Thermo-mechanical Properties

Updated values of the coil properties will be provided as they become available. The properties were based on the MATPRO model used in TRAC code [8].

3.4.1 Property of Nichrome

We assume that Nichrome coils have similar properties with that of Constantan.

(1) Density

A constant value of 8393.4 kg/m3 is used.

(2) Specific heat

The specific heat is $c_p = 110 T_f^{\,0.2075}$,

where c_p is the specific heat (J/kg.K) and T_f is the temperature (F).

(3) Thermal Conductivity

The thermal conductivity is

$k = 29.18 + 2.683x10^{-3}\left(T_f - 100\right)$

where k is the thermal conductivity (W/m.K) and T_f is the temperature (F).

3.4.2 Property of Boron Nitride

(1) Density

A constant value of 2002 kg/m3 is used

(2) Specific Heat

The specific heat is

$c_p = 760.59 + 1.7955T_f - 8.6704x10^{-4}T_f^{\,2} + 1.7955x10^{-7}T_f^{\,3}$,

where c_p is the specific heat (J/kg.K) and T_f is the temperature (F).

(3) Thermal Conductivity

The boron-nitride thermal-conductivity calculation, based on a conversion to SI units of a curve fit is

$k = 25.27 - 1.365 \times 10.3T_f$,

where k is the thermal conductivity (W/m.K) and T_f is the temperature (F).

3.4.3 Property of Inconel 600

(1) Density

The density is:

$\rho = 16.01846 \times (5.261008 \times 10^2 - 1.345453 \times 10^{-2} T_f - 1.194357x10^{-7}T_f^{\,2}$,

where ρ is the density (kg/m^3) and T_f is the temperature (F).

(2) Specific Heat

The specific heat is:

$$c_p = 4186.8\times(0.1014 + 4.378952\times10^{-5}T_f - 2.046138\times10^{-8}T_f{}^2 + 1.7955\times10^{-7}T_f{}^3$$
$$- 2.060318\times10^{-13}T_f{}^4 + 3.682836\times10^{-16}T_f{}^5 - 2.458648\times10^{-19}T_f{}^6 + 5.597571\times10^{-23}T_f{}^7)$$

where c_p is the specific heat (J/kg.K) and T_f is the temperature (F).

(3) Thermal Conductivity

The thermal conductivity is:

$$k = 1.729577\times(8.011332 + 4.643719\times10^{-3}T_f + 1.872857\times10^{-6}T_f{}^2 - 3.914512\times10^{-9}T_f{}^3$$
$$+ 3.475513\times10^{-12}T_f{}^4 - 9.936696\times10^{-16}T_f{}^5)$$

where k is the thermal conductivity (W/m.K) and T_f is the temperature (F).

3.5 Spacer Data

Spacer grids are used to support fuel rods in nuclear reactor fuel assemblies. These grids interact with the flow and heat transfer in a number of ways. It is known that they generally have a beneficial effect on critical heat flux (CHF) in typical nuclear reactor assemblies. However, the obtained enhancement depends on the geometrical characteristics of the spacer grids as well as on the parameter range in terms of pressure, local mass velocity and quality. Spacer grids decrease the flow cross sectional area locally and thereby increase the local velocity pressure drop and heat transfer coefficients. They may have special geometrical features to promote turbulence, the effect of which may propagate further downstream. Spacer grids may provide a larger surface area on which to collect the entrained liquid droplets, which may cause increase in the local fluid film flow rate under sub-CHF conditions and may lead to rewetting of the fuel rod cladding under post-CHF conditions.

There are two types of spacers in this program - ferrule type and grid type. The grid type spacers are applied to the 8x8 assemblies (assemblies 0, 1, 2, and 3). The ferrule type is applied to the high burn-up 8x8 assemblies (assemblies C2A, C2B and C3).

Figures 3.5.1 shows different view of grid spacer design used for assemblies 0, 1, 2, and 3. Figure 3.5.3 shows different views of the ferrule spacer, which was used for the high burn-up fuel assembly designs given as bundles 4, C2A, C2B and C3. These figures and the data for both spacer designs were provided by JNES of Japan.

Using the JNES spacers' data, the spacer grid and ferrule grid dimensions were estimated in co-operation with NEA, OECD as described below. The numeric data was extracted and scaled from the figures using the SigmaScan Pro 5.0 software. The graphical reconstruction was based on the extracted data using 3DsMax 5, PhotoShop and Paint Shop pro 7. The estimated precision of the process used is estimated to be between 2 and 5 percent (1σ) depending on the size of the object measured (the smaller is the object, the higher is the uncertainty since the smaller items are not always exactly to scale). It should be noticed that the graphics made available might have been slightly deformed through the different copying processes therefore it is difficult to be precise on the uncertainty of the data provided. The estimated dimensions and 3D views of the spacers are depicted in Figures 3.5.3 through 3.5.17.

An estimate of the ferrule grid dimensions was performed at PSU. The results are shown in Figure 3.5.18.

In the specification, only bundle average spacer pressure loss coefficients are provided (See Tables 3.2.6 → 3.2.8). Depending on the participants' computer code, and using the provided spaced data, each participant may choose the sub-channel grids loss coefficients or other required input values.

The PSU will provide best-estimate individual sub-channel loss coefficients based on the spacer grid information provided by JNES, for each spacer design. The method used to perform these estimates as well as the best-estimate values will be provided to the participants for their consideration.

Figure 3.5.1 Schematic of the Grid Spacer (dimensions in mm)

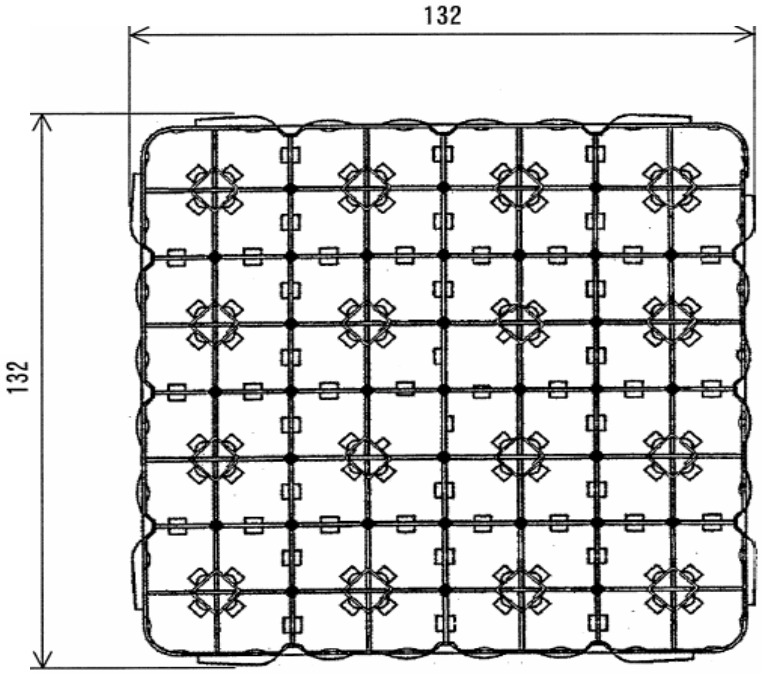

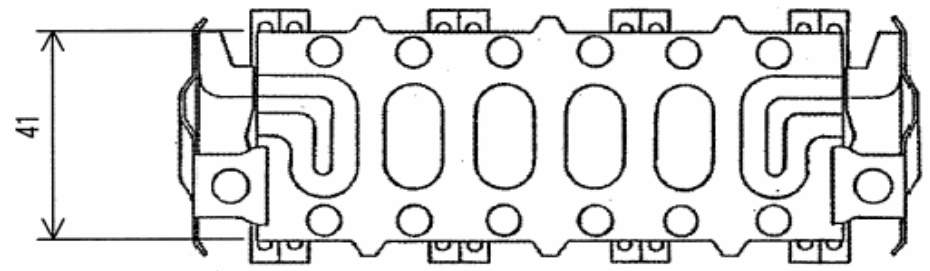

(b) Side View

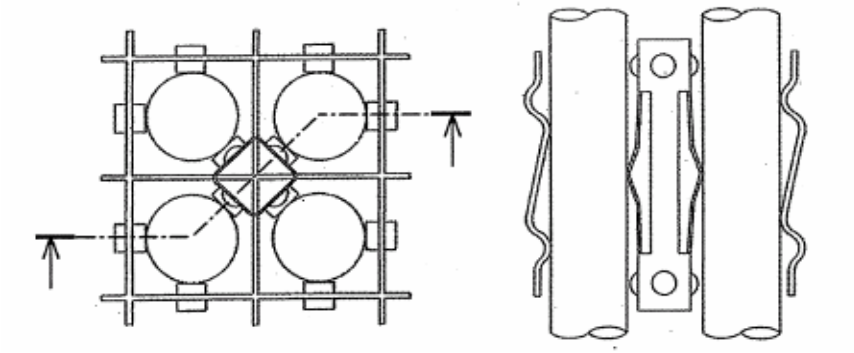

(c) Elementary Structure

Figure 3.5.2 Schematic of Ferrule Spacer Design (dimensions in mm)

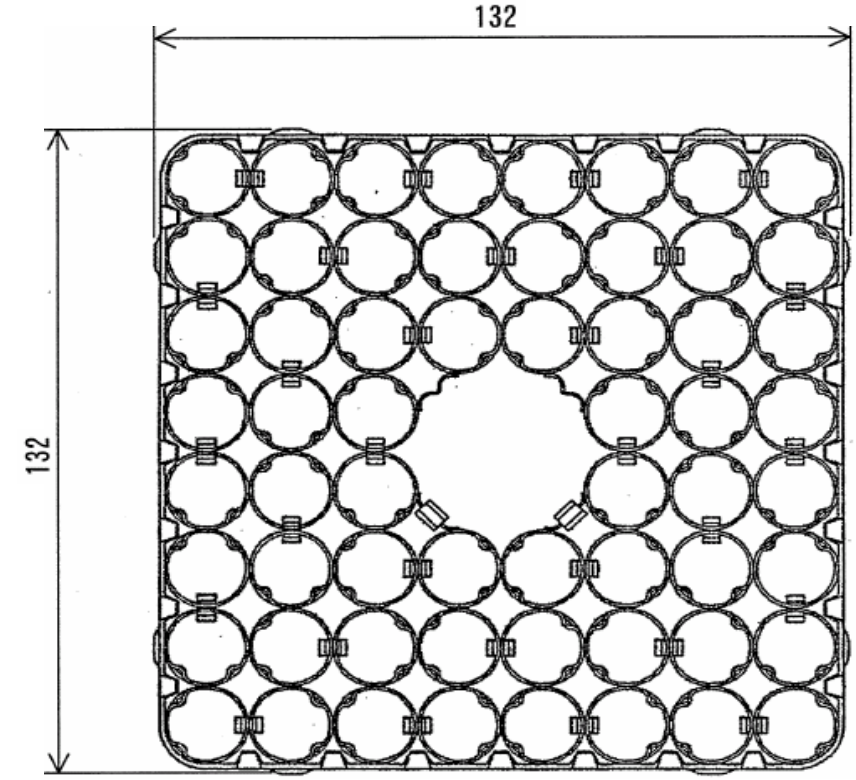

(a) Top View

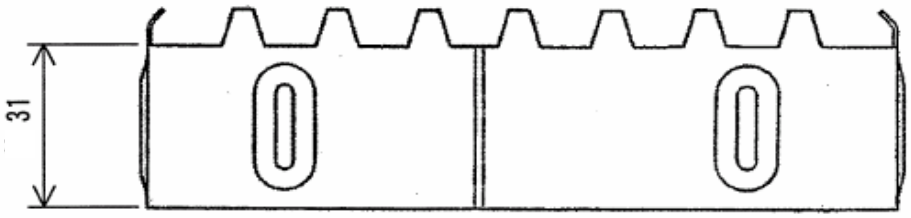

(b) Side View

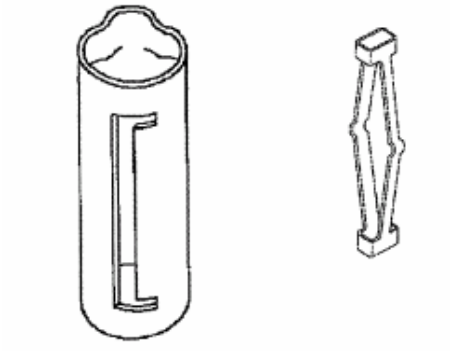

(c) Elementary Structure

Figure 3.5.3 Grid Spacer – Dimensions

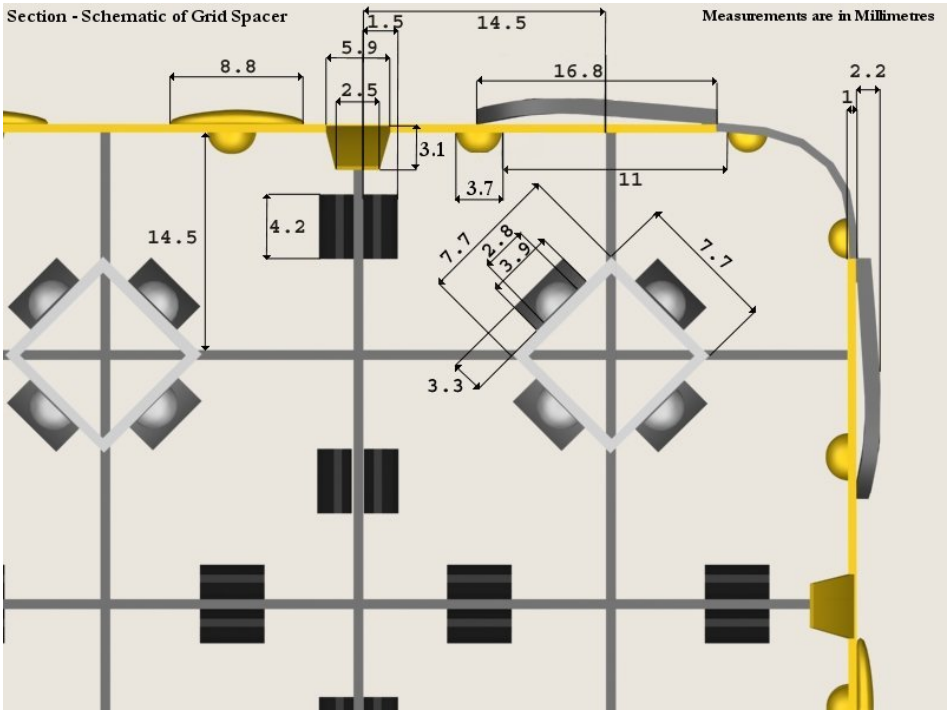

Figure 3.5.4 Grid Spacer – Dimensions

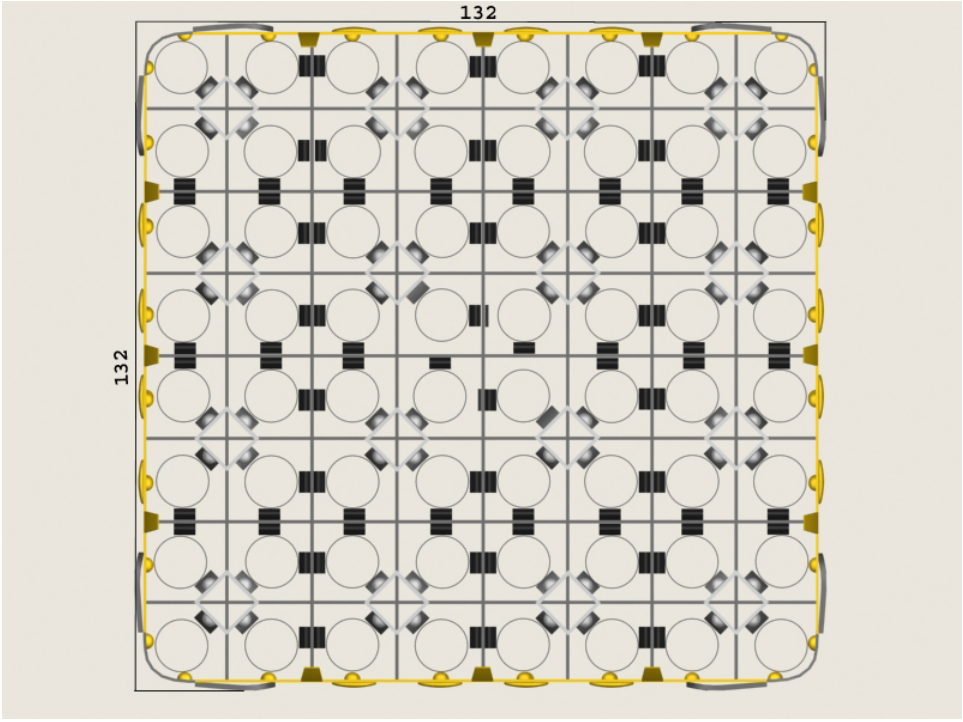

Figure 3.5.5 Grid Spacer – 3D Bottom View

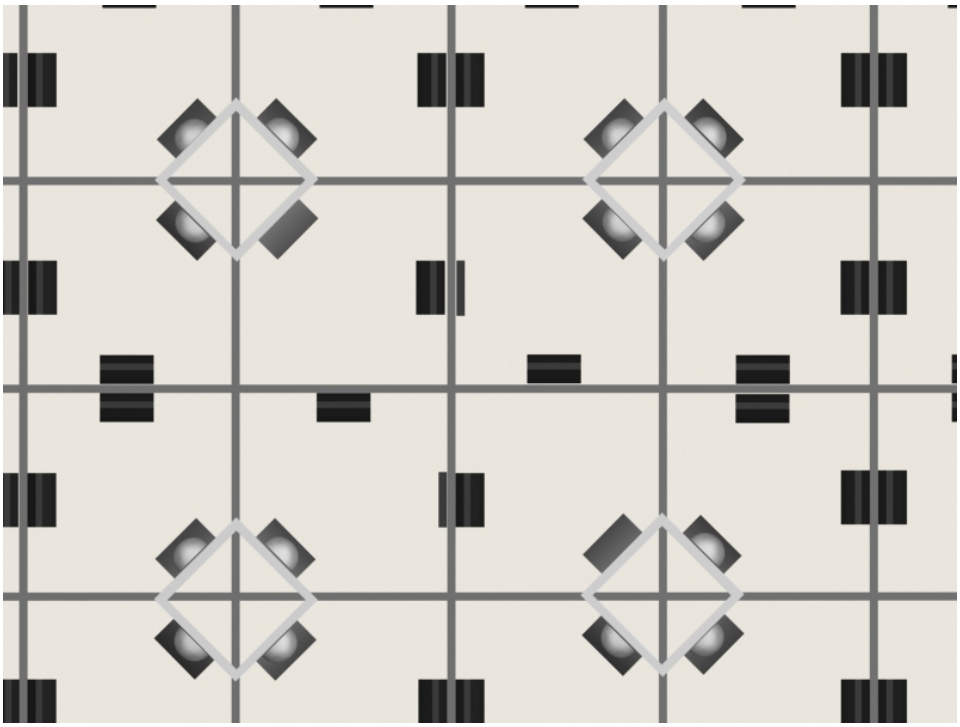

Figure 3.5.6 Grid Spacer – 3D View

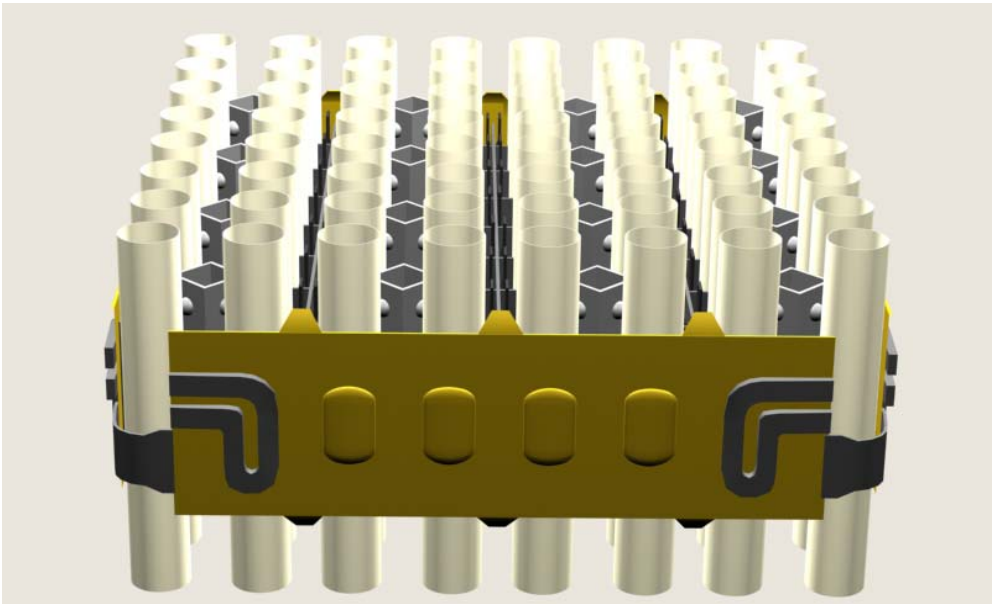

Figure 3.5.7 Grid Spacer – 3D View

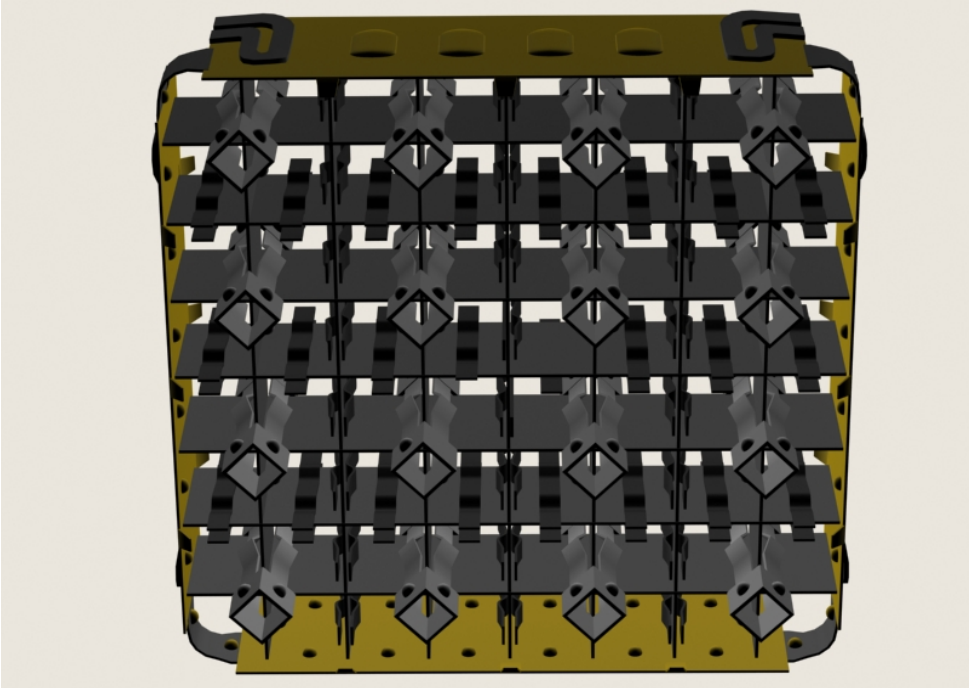

Figure 3.5.8 Grid Spacer – 3D View

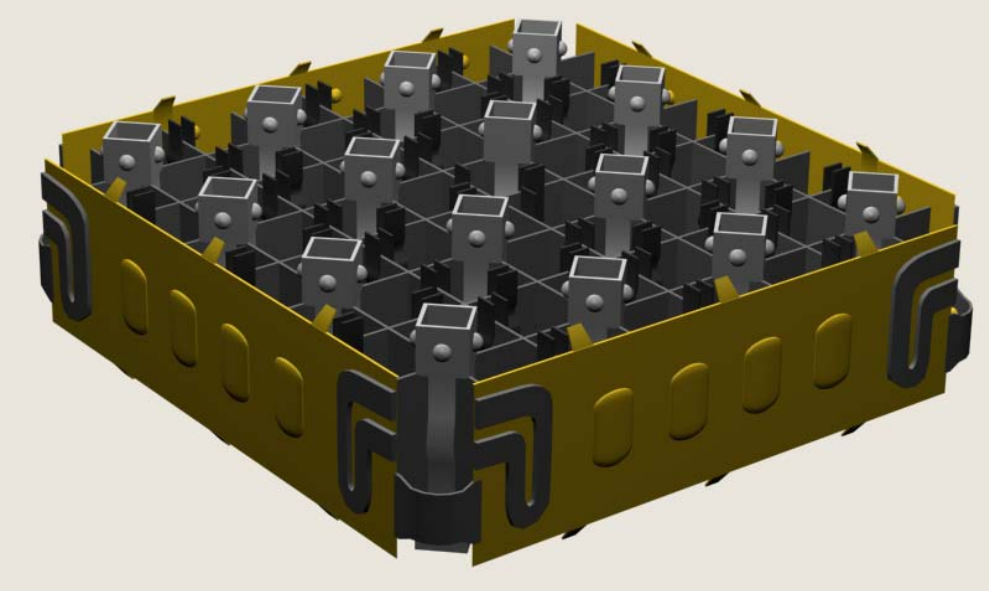

Figure 3.5.9 Grid Spacer – 3D View

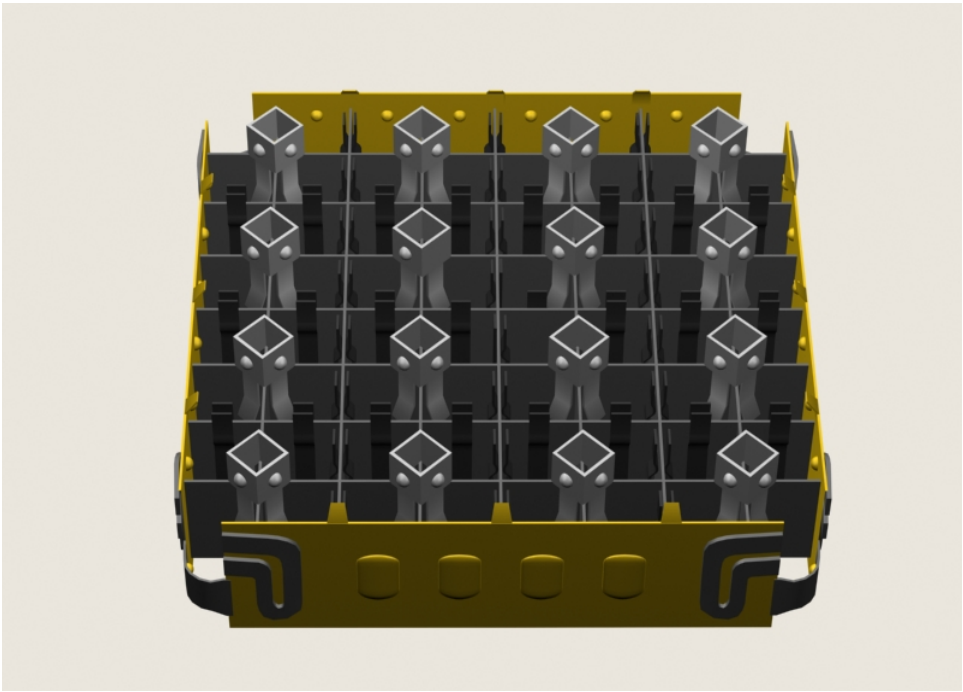

Figure 3.5.10 Grid Spacer – Side View

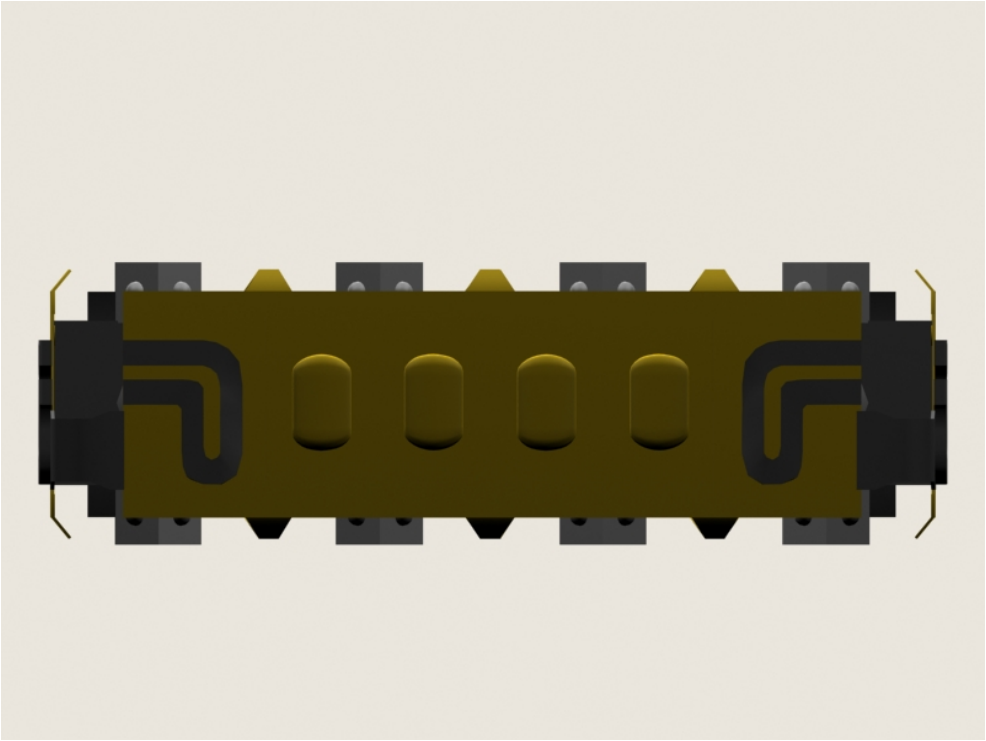

Figure 3.5.11 Grid Spacer – Top View

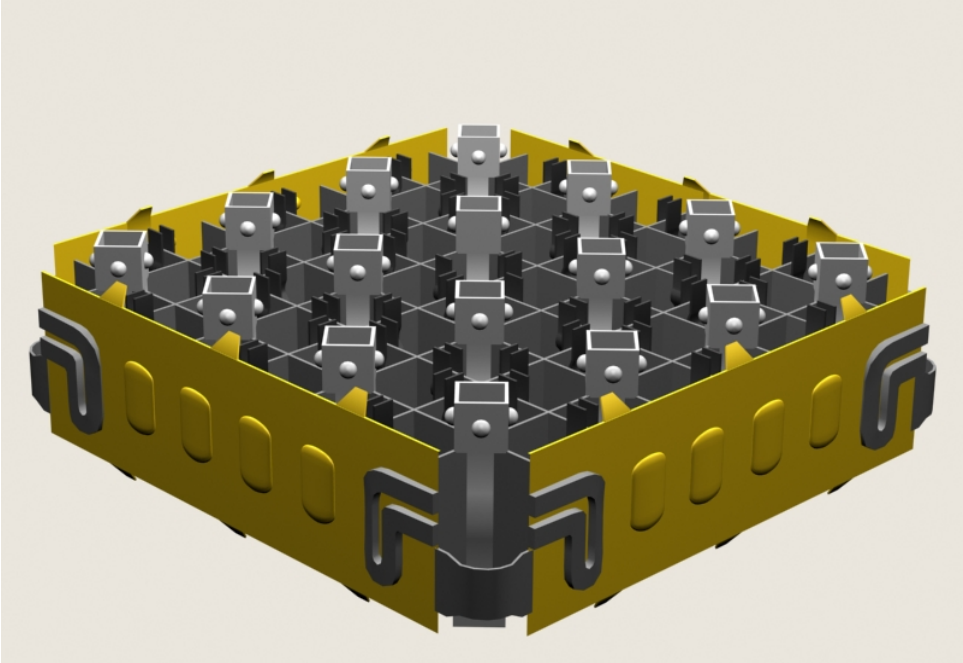

Figure 3.5.12 Grid Spacer – Top Central View

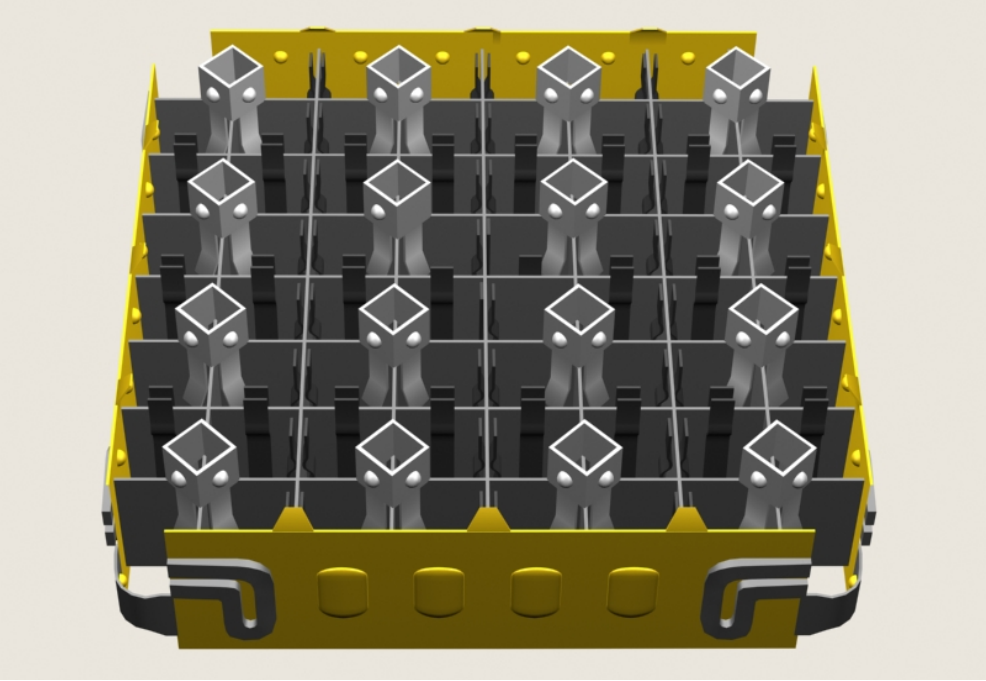

Figure 3.5.13 Ferrule Spacer Design- Dimensions

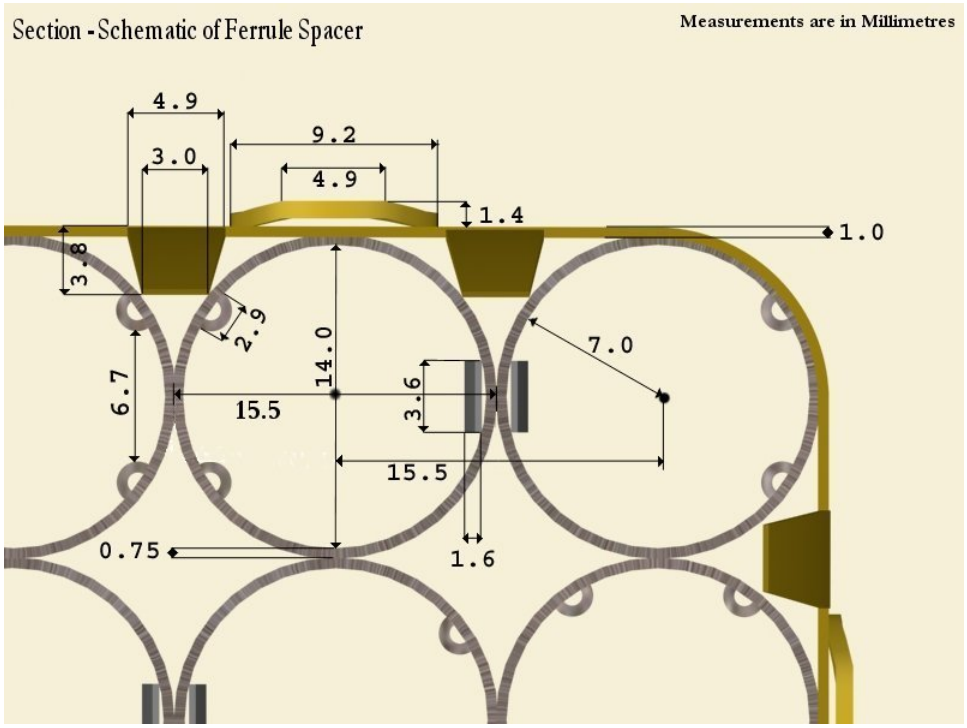

Figure 3.5.14 Ferrule Spacer - 3D View

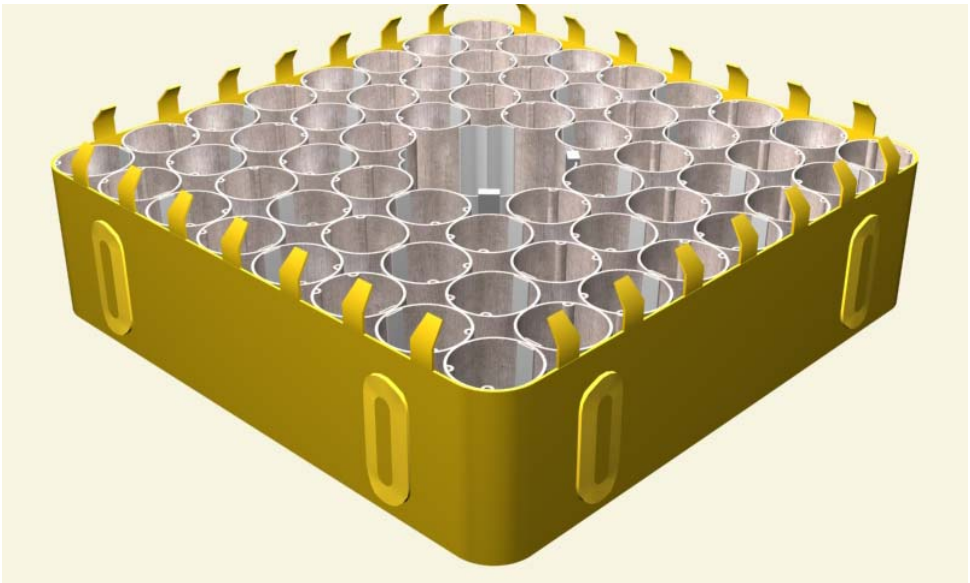

Figure 3.5.15 Ferrule Spacer - 3D View

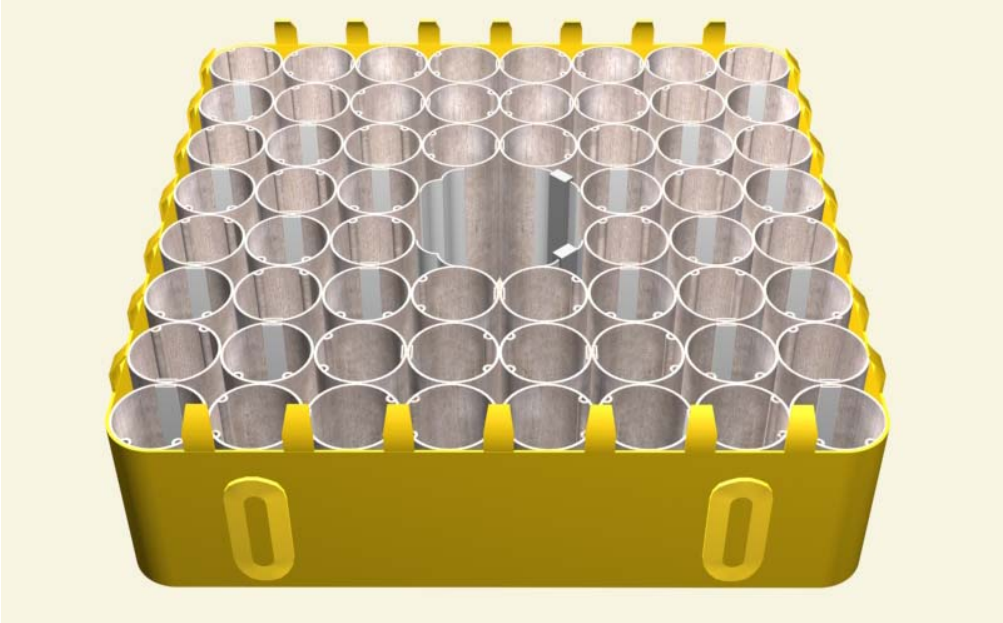

Figure 3.5.16 Ferrule Spacer - Side View

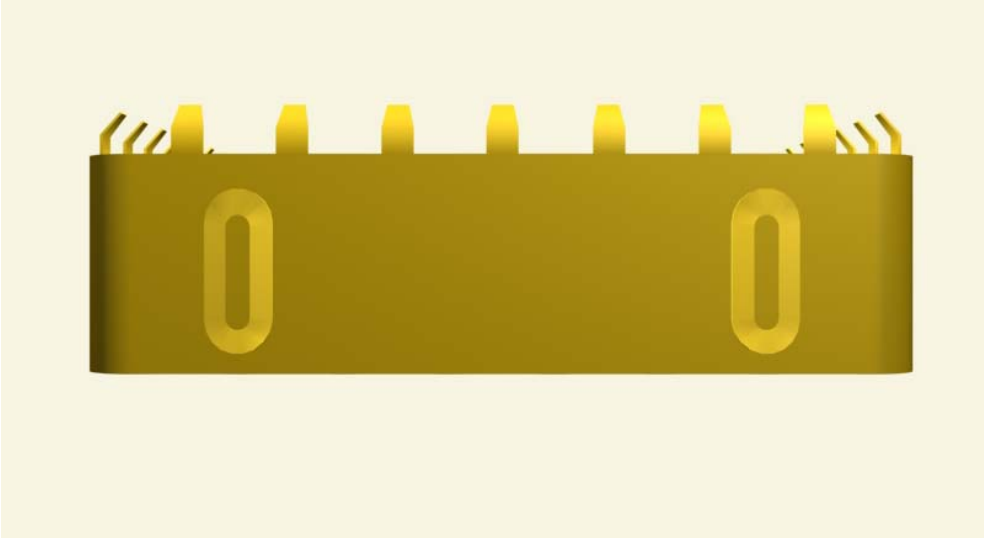

Figure 3.5.17 Ferrule Spacer – Top View

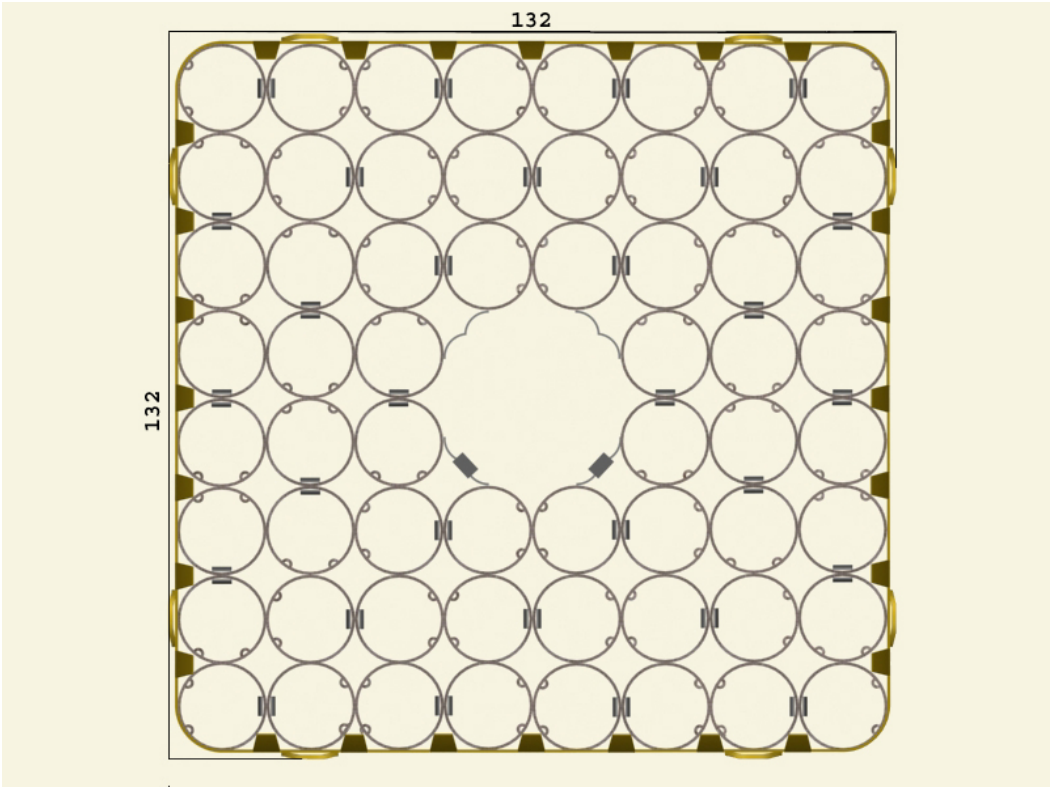

Figure 3.5.18 Schematic of Ferrule Spacer

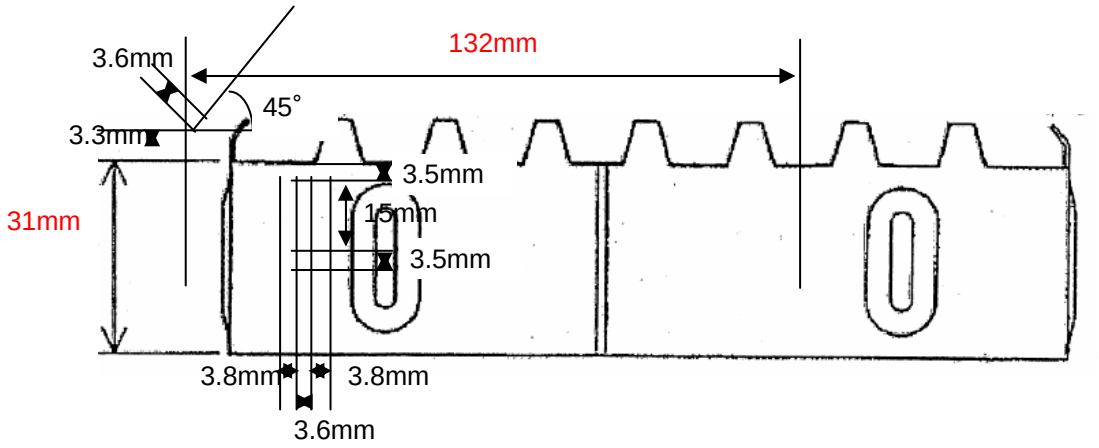

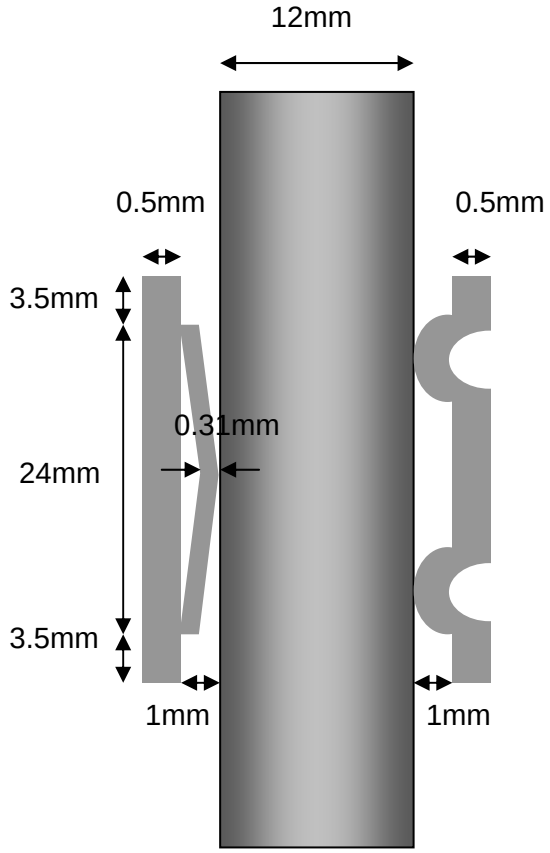

Chapter 4

BENCHMARK DATABASE

4.1 Introduction

A significant amount of data has been collected in the NUPEC BWR full-size mock-up test series. The complete benchmark database for all cases defined in the test matrices is stored on a CD-ROM, which is provided to the participants by NEA/OECD in addition to the Benchmark specification. This chapter describes the complete NUPEC BFBT benchmark database. The data is summarized in Table 4.1.1. Test cases selected for comparative analysis in the framework of the OECD/NRC BFBT benchmark will be described in Chapter 5.

Table 4.1.1 NUPEC BFBT Database

Void Distribution Measurements	**No. of Data Sets**
Steady state void distribution measurements	392
Transient void distribution measurements	2
Critical Power Measurements	**No. of Data Sets**
Single-phase pressure drop measurements	36
Two-phase pressure drop measurements	33
Steady-state critical power measurements	151
Transient critical power measurements	4

4.2 Void distribution measurements

The steady state void distribution measurement initial and boundary nominal conditions are given in Table 4.2.1. The test matrix of steady state void distributions is given in Table 4.2.2 for each assembly type and design. The test numbers of steady state void distribution measurements are given in Table 4.2.3.

Among the major operational transients, the following 4 events were simulated, each one of them with a specific impact on the void distribution:

- Turbine trip without bypass;
- Re-circulation pump trip;
- Re-circulation pump stick;
- Malfunction of pressure control system (pressure vessel).

The transient void distribution measurement conditions are given in Table 4.2.4. The test matrix of transient void distributions is given in Table 4.2.5 and the test numbers are given in Table 4.2.6.

The cases denoted in the tables with E1, E2, and E3 are the ones selected for analysis in Exercises 1 to 3 of the Phase 1 of the BFBT benchmark.

Table 4.2.1 Steady-State Void Distribution Measurement Conditions

Assembly	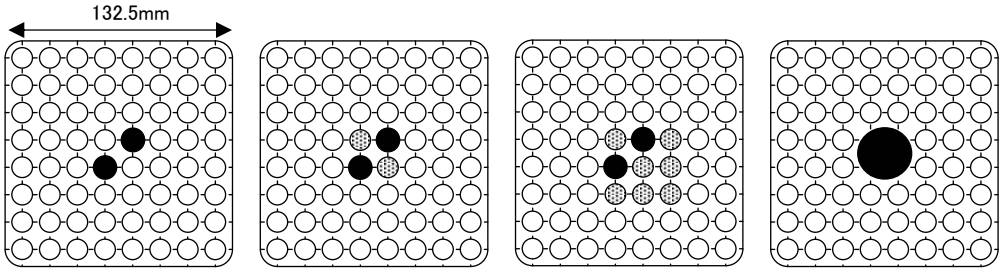	
Boundary Conditions	Pressure (MPa) Flow rate (t/h) Inlet sub-cooling (kJ/kg) Exit quality (%)	7.2 55 50.2 2 5 8 12 18 25
Data	Void distribution matrix in sub-channel mesh size Void distribution matrix in 0.3 × 0.3 mm mesh size (512 × 512 = 262K pixels) Corresponding boundary conditions	
No. of Cases	Data supplied cases Exercise cases	392 sub-channel: 15 microscopic: 3

Exit quality: Thermal equilibrium quality

Table 4.2.2 Test Matrix of Steady-State Void Distribution Measurements

Assembly	Pressure (Mpa)	Inlet sub-cooling (kJ/kg)	Flow rate (t/h)	Exit quality (%)						No. of data
				2	5	8	12	18	25	
0-1	1.0	50.2	10	X	X	X	X	-	-	13
			30	X	X	X	X	-	-	
			55	X	X	W	X	-	-	
	3.9		10	X	X	X	X	X	X	19
			30	X	X	X	X	X	X	
			55	X	X	X	X	X	W	
	7,2	20.9	45	-	X	-	X	-	-	36
		50.2	10	X	X	X	X	X	X	
			20	X	X	X	X	X	X	
			30	X	X	X	X	X	X	
			55	W	E1X	W	E1X	W	E1X	
			70	X	X	X	X	X	-	
		126	55	-	X	-	X	-	-	
	8.6	50.2	10	X	X	X	X	X	X	18
			30	X	X	X	X	X	X	
			55	X	X	X	X	W	-	
0-2	3.9	50.2	55	X	X	X	X	X	W	28
	7.2		10	X	X	X	X	X	X	
			30	X	X	X	X	X	X	
			55	W	E1X	W	E1X	W	E1X	
			70	X	X	X	X	X	-	
	8.6		55	X	X	X	X	W	-	
0-3	3.9	50.2	55	X	X	X	X	X	W	28
	7.2		10	X	X	X	X	X	X	
			30	X	X	X	X	X	X	
			55	W	E1X	W	E1X	W	E1X	
			70	X	X	X	X	X	-	
	8.6		55	X	X	X	X	W	-	
1	1.0	50.2	10	X	X	X	X	-	-	13
			30	X	X	X	X	-	-	
			55	X	X	W	X	-	-	
	3.9		10	X	X	X	X	X	X	19
			30	X	X	X	X	X	X	
			55	X	X	X	X	X	W	
	7,2	20.9	45	-	X	-	X	-	-	36
		50.2	10	X	X	X	X	X	X	
			20	X	X	X	X	X	X	
			30	X	X	X	X	X	X	
			55	W	E1X	W	E1X	W	E1X	
			70	X	X	X	X	X	-	
		126	55	-	X	-	X	-	-	
	8.6	50.2	10	X	X	X	X	X	X	18
			30	X	X	X	X	X	X	
			55	X	X	X	X	W	-	

X: test case, W: duplicated test case, E1: exercise 1 case, E2: exercise 2 case

Table 4.2.2 Test Matrix of Steady-State Void Distribution Measurements (cont'd)

Assembly	Pressure (Mpa)	Inlet sub-cooling (kJ/kg)	Flow rate (t/h)	Exit quality (%)						No. of data
				2	5	8	12	18	25	
2	3.9	50.2	10	X	X	X	X	-	X	14
			30	X	X	X	X	-	-	
			55	X	X	X	X	-	-	
	7.2		10	X	X	X	X	-	X	23
			20	X	X	X	X	-	X	
			30	X	X	X	X	-	X	
			55	X	X	X	W	-	-	
			70	X	X	X	-	-	-	
	8.6		10	X	X	X	X	-	X	13
			30	X	X	X	X	-	-	
			55	X	X	W	-	-	-	
3	3.9	50.2	55	X	X	X	X	X	W	28
	7.2		10	X	X	X	X	X	X	
			30	X	X	X	X	X	X	
			55	W	X	W	X	W	X	
			70	X	X	X	X	X	-	
	8.6		55	X	X	X	X	W	-	
4	1.0	50.2	10	X	X	X	X	-	-	13
			30	X	X	X	X	-	-	
			55	X	X	W	X	-	-	
	3.9		10	X	X	X	X	X	X	19
			30	X	X	X	X	X	X	
			55	X	X	X	X	X	W	
	7,2	20.9	45	-	X	-	X	-	-	36
		50.2	10	X	X	X	X	X	X	
			20	X	X	X	X	X	X	
			30	X	X	X	X	X	X	
			55	W	E1E2X	W	E1E2X	W	E1E2X	
			70	X	X	X	X	X	-	
		126	55	-	X	-	X	-	-	
	8.6	50.2	10	X	X	X	X	X	X	18
			30	X	X	X	X	X	X	
			55	X	X	X	X	W	-	

X: test case, W: duplicated test case, E1: case for exercise 1, E2: case for exercise 2

Table 4.2.3 Test No. of Steady-State Void Distribution Measurements(Note)

Test No.	Assembly	Pressure (Mpa)	Flow rate (t/h)	Inlet sub-cooling (kJ/kg)	Exit quality (%)	Exercise cases	
0011-53	0-1	7.18	54.5	51.5	2.0	-	-
0011-54	0-1	7.17	54.2	52.3	1.9	-	-
0011-55	0-1	7.18	54.0	52.6	5.0	E1	-
0011-56	0-1	7.17	54.8	51.6	7.8	-	-
0011-57	0-1	7.16	54.8	49.8	8.0	-	-
0011-58	0-1	7.17	54.9	51.0	12.0	E1	-
0011-59	0-1	7.18	54.8	50.2	17.9	-	-
0011-60	0-1	7.19	55.0	52.1	18.0	-	-
0011-61	0-1	7.21	54.8	50.9	24.9	E1	-
0021-15	0-2	7.16	54.7	52.3	1.9	-	-
0021-16	0-2	7.19	54.9	54.0	4.8	E1	-
0021-17	0-2	7.17	54.8	51.1	7.9	-	-
0021-18	0-2	7.17	54.9	49.8	12.1	E1	-
0021-19	0-2	7.17	54.9	49.4	18.0	-	-
0021-20	0-2	7.16	54.8	51.5	17.8	-	-
0021-21	0-2	7.18	54.9	51.4	24.9	E1	-
0031-15	0-3	7.17	55.0	52.3	1.9	-	-
0031-16	0-3	7.18	55.0	52.4	4.9	E1	-
0031-17	0-3	7.16	54.8	50.5	8.0	-	-
0031-18	0-3	7.18	54.8	50.0	12.1	E1	-
0031-19	0-3	7.17	54.8	50.8	18.0	-	-
0031-20	0-3	7.16	54.8	49.6	18.0	-	-
0031-21	0-3	7.17	54.9	49.4	25.0	E1	-
1071-53	1	7.18	54.6	52.2	1.9	-	-
1071-54	1	7.17	54.4	52.4	1.9	-	-
1071-55	1	7.19	54.6	52.8	4.9	E1	-
1071-56	1	7.20	54.6	54.0	7.9	-	-
1071-57	1	7.17	54.6	52.3	7.9	-	-
1071-58	1	7.16	55.1	50.3	11.9	E1	-
1071-59	1	7.18	54.7	51.3	18.0	-	-
1071-60	1	7.18	55.0	51.8	17.9	-	-
1071-61	1	7.20	54.7	51.8	25.1	E1	-
4101-53	4	7.18	54.7	52.8	1.9	-	-
4101-54	4	7.19	54.6	52.7	1.9	-	-
4101-55	4	7.20	54.6	52.9	5.0	E1	E2
4101-56	4	7.17	54.6	51.8	7.9	-	-
4101-57	4	7.17	54.6	52.4	8.0	-	-
4101-58	4	7.15	54.6	50.6	12.1	E1	E2
4101-59	4	7.19	54.6	52.1	18.1	-	-
4101-60	4	7.18	54.6	50.5	18.2	-	-
4101-61	4	7.18	54.7	52.5	25.1	E1	E2

E1: case for exercise 1, E2: case for exercise 2

(Note) Cases listed in Table 4.2.3 are a part of cases in the matrix shown in Table 4.2.2.

Table 4.2.4 Transient Void Distribution Measurement Conditions

Assembly	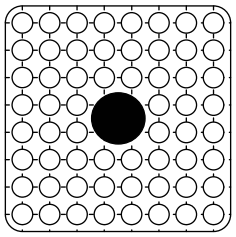 4	
Rated Initial Conditions	Pressure (MPa) Power (MW) Flow rate (t/h) Inlet temperature (Celsius)	7.2 4.5 55 279
Transients	Turbine trip without bypass Re-circulation pump trip	
Data	Time histories of cross sectional averaged void fraction in each axial level during transients Corresponding boundary conditions during transients	
No. of Cases	Data supplied cases Exercise cases	2

Table 4.2.5 Test Matrix of Transient Void Distribution Measurements

Assembly	Initial Conditions				Transients	Exercise cases	No. of Cases
	Pressure (Mpa)	Power (MW)	Flow rate (t/h)	Inlet temperature (Celsius)			
4	7.2	4.5	55	279	Turbine trip without bypass	E3	2
					Re-circulation pump trip	E3	

E3: case for exercise 3

Table 4.2.6 Test No. of Transient Void Distribution Measurements

Test No.	Assembly	Initial Conditions				Transients	Exercise cases
		Pressure (Mpa)	Power (MW)	Flow rate (t/h)	Inlet temperature (Celsius)		
4102-001~009	4	7.2	4.5	55	279	Turbine trip without bypass	E3
4102-019~027	4	7.2	4.5	55	279	Re-circulation pump trip	E3

E3: exercise 3 case

4.3 Critical power measurements

The single-phase pressure drop measurement conditions are given in Table 4.3.1 for bundle design 4. Table 4.3.2 shows the test matrix of single-phase pressure drop measurements. The test numbers of single phase pressure drop conditions are given in Table 4.3.3. The two-phase pressure drop measurement conditions are provided in Table 4.3.4 for bundle configuration C2A. The Table 4.3.5 presents the test matrix of two-phase pressure drop measurements. The test numbers of two phase pressure drop measurements are given in Table 4.3.6. The steady state critical power measurement conditions are provided in Table 4.3.7 for the different bundle designs. The test matrix of steady state critical power measurements is presented in Table 4.3.8 while the test numbers of steady state critical power measurements are shown for assembly C2A, C2B and C3 in Tables 4.3.9 through 4.3.11. The transient boiling transition measurement conditions are given in Table 4.3.12 for the different bundles. The test matrix of transient boiling transition measurements is provided in Table 4.3.13. The test numbers of transient boiling transition measurements are shown in Table 4.3.14.

The cases denoted in the tables with E are the ones selected for analysis in Exercises 1 and 2 of the Phase 2 of the BFBT benchmark.

Table 4.3.1 Single-Phase Pressure Drop Measurement Conditions

Assembly	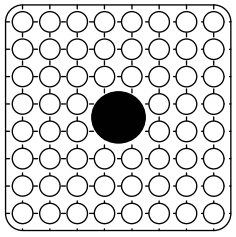 C2	
Boundary Conditions	Pressure (MPa) Flow rate (t/h)	0.1 0.98 7.2 10 15 20 25 30 35 40 45 55 60 65 70
Data	Pressure drop along with axial heated length Corresponding boundary conditions	
No. of Cases	Data supplied cases Exercise cases	36
Concerned Issues	Single-phase pressure drop from bottom to top of heated length	

Table 4.3.2 Test Matrix of Single-Phase Pressure Drop Measurements

Assembly	Pressure (Mpa)	Flow rate (t/h)												No. of data
		10	15	20	25	30	35	40	45	55	60	65	70	
C2A	0.1	X	X	X	X	X	X	X	X	X	X	X	X	36
	1.0	X	X	X	X	X	X	X	X	X	X	X	X	
	7.2	X	X	X	X	X	X	X	X	X	X	X	X	

X: test case, E: case for exercise

Table 4.3.3 Test No. of Single-Phase Pressure Drop Measurements

Test No.	Assembly	Pressure (Mpa)	Flow rate (t/h)	Exercise cases
P70001	C2A	0.2	9.9	-
P70002	C2A	0.2	14.5	-
P70003	C2A	0.2	19.9	-
P70004	C2A	0.2	24.9	-
P70005	C2A	0.2	29.8	-
P70006	C2A	0.2	34.8	-
P70007	C2A	0.2	39.7	-
P70008	C2A	0.2	44.8	-
P70009	C2A	0.2	54.6	-
P70010	C2A	0.2	59.8	-
P70011	C2A	0.2	64.2	-
P70012	C2A	0.2	69.2	-
P70013	C2A	1.0	9.9	-
P70014	C2A	0.99	14.9	-
P70015	C2A	0.99	20.3	-
P70016	C2A	0.98	24.8	-
P70017	C2A	0.98	29.9	-
P70018	C2A	0.99	34.7	-
P70019	C2A	0.99	39.8	-
P70020	C2A	0.99	45.3	-
P70021	C2A	1.0	54.8	-
P70022	C2A	0.98	59.8	-
P70023	C2A	0.98	64.8	-
P70024	C2A	0.98	69.8	-
P70025	C2A	7.17	9.9	-
P70026	C2A	7.15	15.4	-
P70027	C2A	7.15	20.3	-
P70028	C2A	7.16	24.9	-
P70029	C2A	7.16	29.8	-
P70030	C2A	7.16	34.7	-
P70031	C2A	7.16	39.7	-
P70032	C2A	7.16	44.6	-
P70033	C2A	7.15	55.0	-
P70034	C2A	7.15	59.7	-
P70035	C2A	7.16	64.8	-
P70036	C2A	7.15	69.9	-

E: exercise case

Table 4.3.4 Two-Phase Pressure Drop Measurement Conditions

Assembly	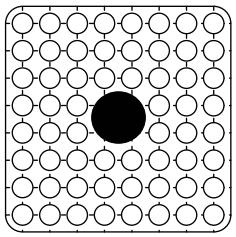 C2A	
Boundary Conditions	Pressure (MPa) Flow rate (t/h) Inlet sub-cooling (kJ/kg) Exit quality (%)	7.2 8.6 20 45 55 70 50.2 7 10 15 20 25
Data	Pressure drop along with axial heated length Corresponding boundary conditions	
No. of Cases	Data supplied cases Exercise cases	33

Exit quality: Thermal equilibrium quality

Table 4.3.5 Test Matrix of Two-Phase Pressure Drop Measurements

Assembly	Pressure (Mpa)	Flow rate (t/h)	Inlet sub-cooling (kJ/kg)	Exit quality (%)					No. of data
				7	10	15	20	25	
C2A	7.2	20	50.2	X	X	X	X	W	21
		45		X	X	X	X	X	
		55		X	X	X	X	W	
		70		X	X	X	X	-	
	8.6	20	50.2	X	-	X	-	X	12
		45		X	-	X	-	X	
		55		X	-	X	-	W	
		70		X	-	X	-	-	

X: test case, W: duplicated test case, E: exercise case

Table 4.3.6 Test Number (No.) of Two-Phase Pressure Drop Measurements

Test No.	Assembly	Pressure (Mpa)	Flow rate (t/h)	Inlet sub-cooling (kJ/kg)	Exit quality (%)	Exercise cases
P60001	C2A	7.16	20.2	53.3	6.7	-
P60002	C2A	7.16	20.1	51.8	9.9	-
P60003	C2A	7.16	20.1	50.8	14.8	-
P60004	C2A	7.16	20.2	51.3	19.9	-
P60005	C2A	7.16	20.0	51.1	24.9	-
P60006	C2A	7.16	20.1	50.8	24.9	-
P60007	C2A	7.17	55.0	51.1	7.0	-
P60008	C2A	7.17	55.0	49.0	10.1	-
P60009	C2A	7.17	55.0	51.1	15.0	-
P60010	C2A	7.17	54.9	47.3	20.1	-
P60011	C2A	7.17	54.9	50.6	25.1	-
P60012	C2A	7.17	55.0	49.7	25.1	-
P60013	C2A	7.16	69.9	47.2	7.3	-
P60014	C2A	7.16	70.1	50.6	10.0	-
P60015	C2A	7.17	70.0	49.5	15.1	-
P60016	C2A	7.18	70.1	50.3	20.0	-
P60017	C2A	7.16	45.1	51.0	6.8	-
P60018	C2A	7.17	44.9	50.8	10.0	-
P60019	C2A	7.17	45.0	49.4	15.1	-
P60020	C2A	7.16	45.1	51.8	19.8	-
P60021	C2A	7.16	45.1	50.8	25.0	-
P60022	C2A	8.64	20.2	50.7	7.0	-
P60023	C2A	8.63	20.2	52.3	14.8	-
P60024	C2A	8.63	20.2	52.9	24.9	-
P60025	C2A	8.64	55.0	51.3	6.9	-
P60026	C2A	8.64	55.1	53.0	14.7	-
P60027	C2A	8.64	55.1	51.5	24.9	-
P60028	C2A	8.63	55.1	51.3	24.9	-
P60029	C2A	8.64	70.1	51.5	6.9	-
P60030	C2A	8.64	70.2	51.4	14.9	-
P60031	C2A	8.64	45.1	53.0	6.9	-
P60032	C2A	8.63	45.2	51.3	14.9	-
P60033	C2A	8.63	45.1	51.6	24.9	-

E: exercise case

Table 4.3.7 Critical Power Measurement Conditions

Assembly	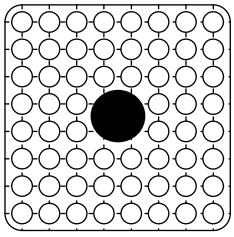 C2A	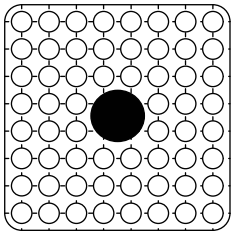 C2B 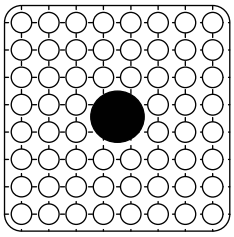 C3
Boundary Conditions	Pressure (MPa) Flow rate (t/h) Inlet sub-cooling (kJ/kg)	5.5 7.2 8.6 10 20 30 45 55 60 65 25 50 84 104 126
Data	Critical power, Location of boiling transition Corresponding boundary conditions	
No. of Cases	Data supplied cases Exercise cases	151 44

Table 4.3.8 Test Matrix of Critical Power Measurements

Assembly	Pressure (Mpa)	Flow rate (t/h)	Inlet sub-cooling (kJ/kg)					No. of data
			25	50	84	104	126	
C2A	5.5	20	X	EW	X	-	X	20
		45	X	EX	X	-	X	
		55	EW	EW	EW	-	EX	
		65	X	EX	X	-	X	
	7.2	10	X	X	X	X	X	35
		20	X	EW	X	X	X	
		30	X	EX	X	X	X	
		45	X	EX	X	X	X	
		55	EW	EW	EX	EW	EX	
		60	X	EX	X	X	X	
		65	X	EX	X	X	X	
	8.6	20	X	EW	X	-	X	20
		45	X	EX	X	-	X	
		55	EW	EW	EW	-	EX	
		65	X	EX	X	-	X	
C2B	7.2	10	X	X	X	X	X	36
		20	X	EX	X	X	X	
		30	X	EX	X	X	X	
		45	X	EX	X	X	X	
		55	EX	EW	EX	EX	EX	
		60	X	EX	X	X	X	
		65	X	EX	X	X	X	
C3	7.2	10	X	X	X	X	X	36
		20	X	EX	X	X	X	
		30	X	EX	X	X	X	
		45	X	EX	X	X	X	
		55	EX	EW	EX	EX	EX	
		60	X	EX	X	X	X	
		65	X	EX	X	X	X	

X: test case, W: duplicated test case, E: exercise case

Table 4.3.9 Test Numbers (No.) of Critical Power Measurements (C2A)

Test No.	Assembly	Pressure (Mpa)	Flow rate (t/h)	Inlet sub-cooling (kJ/kg)	Exercise cases
SA505500	C2A	5.49	20.16	50.95	E
SA505501	C2A	5.49	20.10	51.35	E
SA505600	C2A	5.51	20.12	84.79	-
SA505800	C2A	5.50	20.19	129.38	-
SA505900	C2A	5.49	20.14	26.04	-
SA510500	C2A	5.48	55.06	56.41	E
SA510501	C2A	5.51	55.11	62.48	E
SA510600	C2A	5.51	54.70	96.16	E
SA510601	C2A	5.52	55.34	96.79	E
SA510800	C2A	5.51	54.81	134.97	E
SA510900	C2A	5.52	54.70	35.33	E
SA510901	C2A	5.51	55.05	35.02	E
SA512500	C2A	5.54	65.48	64.36	E
SA512600	C2A	5.51	64.97	99.60	-
SA512800	C2A	5.50	65.52	133.75	-
SA512900	C2A	5.52	65.12	40.30	-
SA516500	C2A	5.51	44.85	55.98	E
SA516600	C2A	5.52	45.03	91.83	-
SA516800	C2A	5.50	45.28	132.07	-
SA516900	C2A	5.52	45.13	35.66	-
SA603500	C2A	7.18	10.07	51.85	-
SA603600	C2A	7.16	10.07	86.12	-
SA603700	C2A	7.17	9.98	106.75	-
SA603800	C2A	7.16	9.99	122.79	-
SA603901	C2A	7.18	10.01	25.82	-
SA605500	C2A	7.16	20.09	50.55	E
SA605502	C2A	7.17	20.07	51.44	E
SA605600	C2A	7.17	20.19	83.57	-
SA605700	C2A	7.17	20.24	106.22	-
SA605801	C2A	7.16	20.21	127.20	-
SA605900	C2A	7.16	20.21	22.61	-
SA607500	C2A	7.13	30.02	48.35	E
SA607600	C2A	7.15	30.23	82.55	-
SA607700	C2A	7.16	30.00	106.63	-
SA607800	C2A	7.18	30.12	126.80	-
SA607900	C2A	7.15	30.23	23.42	-
SA610503	C2A	7.17	55.20	59.39	E
SA610504	C2A	7.17	55.47	58.09	E
SA610600	C2A	7.18	55.05	89.53	E
SA610700	C2A	7.13	55.20	107.61	E
SA610701	C2A	7.21	54.88	113.28	E
SA610800	C2A	7.24	55.30	137.26	E
SA610900	C2A	7.27	55.10	37.73	E
SA610902	C2A	7.18	55.42	32.94	E
SA611500	C2A	7.13	60.23	54.89	E
SA611600	C2A	7.12	60.18	89.39	-
SA611700	C2A	7.23	60.10	114.29	-

E: exercise case

Table 4.3.9 Test Numbers (No.) of Critical Power Measurements (C2A) (cont'd)

Test No.	Assembly	Pressure (Mpa)	Flow rate (t/h)	Inlet sub-cooling (kJ/kg)	Exercise cases
SA611800	C2A	7.15	60.07	131.68	-
SA611900	C2A	7.16	60.30	33.18	-
SA612500	C2A	7.16	65.36	55.66	E
SA612600	C2A	7.17	64.99	91.82	-
SA612700	C2A	7.17	65.19	107.82	-
SA612800	C2A	7.18	65.01	132.81	-
SA612900	C2A	7.16	65.72	32.31	-
SA616500	C2A	7.13	45.17	54.21	E
SA616600	C2A	7.19	45.01	88.72	-
SA616700	C2A	7.23	45.13	110.60	-
SA616800	C2A	7.15	45.07	128.01	-
SA616900	C2A	7.14	45.35	30.59	-
SA805500	C2A	8.63	20.30	51.00	E
SA805501	C2A	8.64	20.30	50.28	E
SA805600	C2A	8.62	20.26	82.58	-
SA805800	C2A	8.60	20.31	125.79	-
SA805900	C2A	8.63	20.13	27.84	-
SA810501	C2A	8.62	55.15	54.89	E
SA810502	C2A	8.64	55.16	55.12	E
SA810600	C2A	8.56	55.00	83.85	E
SA810601	C2A	8.64	55.21	88.54	E
SA810800	C2A	8.64	55.28	130.30	E
SA810900	C2A	8.66	55.38	30.97	E
SA810901	C2A	8.60	55.15	27.55	E
SA812500	C2A	8.64	65.25	58.08	E
SA812600	C2A	8.64	64.95	91.08	-
SA812800	C2A	8.67	65.27	135.52	-
SA812900	C2A	8.65	65.22	29.55	-
SA816500	C2A	8.61	45.24	52.22	E
SA816600	C2A	8.67	45.52	88.65	-
SA816800	C2A	8.60	45.23	128.18	-
SA816900	C2A	8.65	45.24	27.81	-

E: exercise case

Table 4.3.10 Test numbers (No.) Critical Power measurements (C2B)

Run No.	Assembly	Pressure (Mpa)	Flow rate (t/h)	Inlet sub-cooling (kJ/kg)	Exercise cases
SB603500	C2B	7.17	9.93	50.50	-
SB603602	C2B	7.15	9.96	84.59	-
SB603700	C2B	7.17	9.99	104.90	-
SB603800	C2B	7.15	10.09	128.57	-
SB603900	C2B	7.14	10.01	23.14	-
SB605500	C2B	7.15	20.03	51.66	E
SB605600	C2B	7.14	19.93	80.09	-
SB605700	C2B	7.16	20.18	103.88	-
SB605800	C2B	7.17	20.07	126.40	-
SB605900	C2B	7.14	19.84	21.06	-
SB607500	C2B	7.13	30.05	49.90	E
SB607600	C2B	7.17	29.95	83.37	-
SB607700	C2B	7.16	29.83	105.04	-
SB607800	C2B	7.14	29.97	126.27	-
SB607900	C2B	7.18	29.76	24.61	-
SB610500	C2B	7.2	54.84	54.28	E
SB610501	C2B	7.19	54.91	51.16	E
SB610600	C2B	7.18	54.91	82.45	E
SB610700	C2B	7.18	54.71	105.31	E
SB610800	C2B	7.14	54.90	122.48	E
SB610900	C2B	7.2	54.88	26.55	E
SB611500	C2B	7.19	59.88	54.03	E
SB611600	C2B	7.19	59.95	87.15	-
SB611700	C2B	7.13	59.74	101.34	-
SB611800	C2B	7.18	59.88	127.26	-
SB611900	C2B	7.13	59.83	26.83	-
SB612500	C2B	7.18	64.60	48.65	E
SB612600	C2B	7.18	64.68	81.47	-
SB612700	C2B	7.21	64.05	106.23	-
SB612800	C2B	7.15	64.82	125.63	-
SB612900	C2B	7.16	64.85	21.18	-
SB616501	C2B	7.14	44.82	47.96	E
SB616600	C2B	7.18	44.91	83.57	-
SB616700	C2B	7.18	44.93	107.37	-
SB616800	C2B	7.16	45.01	127.09	-
SB616900	C2B	7.18	44.82	27.54	-

E: exercise case

Table 4.3.11 Test numbers (No.) Critical Power Measurements (C3)

Test No.	Assembly	Pressure (Mpa)	Flow rate (t/h)	Inlet sub-cooling (kJ/kg)	Exercise cases
SC603900	C3	7.14	9.95	21.70	-
SC603500	C3	7.15	9.95	50.88	-
SC603600	C3	7.16	10.01	88.57	-
SC603700	C3	7.17	9.93	105.55	-
SC603800	C3	7.16	9.98	125.35	-
SC605900	C3	7.12	19.95	22.11	-
SC605500	C3	7.16	19.96	50.40	E
SC605600	C3	7.15	19.86	80.19	-
SC605700	C3	7.13	19.93	102.45	-
SC605800	C3	7.15	19.91	125.18	-
SC607900	C3	7.17	29.88	23.62	-
SC607500	C3	7.15	29.83	51.09	E
SC607600	C3	7.15	29.92	82.80	-
SC607701	C3	7.15	29.91	105.59	-
SC607800	C3	7.10	29.99	122.82	-
SC616900	C3	7.13	44.93	22.94	-
SC616500	C3	7.15	45.04	50.88	E
SC616600	C3	7.14	44.95	82.80	-
SC616701	C3	7.12	44.91	102.89	-
SC616800	C3	7.14	44.89	123.57	-
SC610900	C3	7.19	54.90	31.35	E
SC610500	C3	7.19	54.90	50.74	E
SC610502	C3	7.14	54.76	49.84	E
SC610600	C3	7.13	54.66	81.93	E
SC610700	C3	7.15	54.83	103.37	E
SC610800	C3	7.21	55.06	128.69	E
SC611900	C3	7.14	59.97	25.27	-
SC611500	C3	7.19	59.72	51.05	E
SC611600	C3	7.13	59.91	81.73	-
SC611700	C3	7.19	59.91	104.96	-
SC611800	C3	7.15	59.78	124.09	-
SC612900	C3	7.15	64.99	24.40	-
SC612500	C3	7.17	65.02	52.32	E
SC612600	C3	7.17	64.87	84.39	-
SC612700	C3	7.16	64.86	104.64	-
SC612800	C3	7.16	64.87	125.74	-

E: exercise case

Table 4.3.12 Transient Boiling Transition Measurement Conditions

Assembly	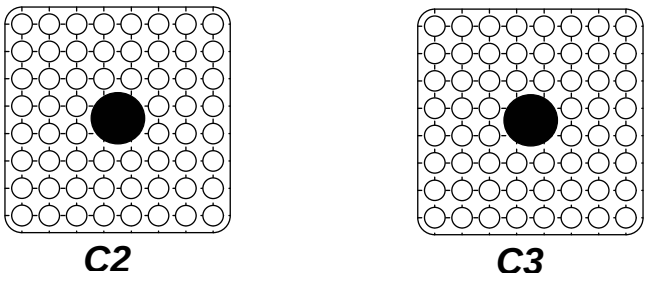	
Rated Initial Conditions	Pressure (MPa) Power (MW) Flow rate (t/h) Inlet enthalpy (kJ/kg)	7.2 6.2~8.5 45 1217~1227
Transients	Turbine trip without bypass Re-circulation pump trip	
Data	Time histories of cladding temperature where boiling transition occurred Timing of boiling transition, Timing of rewetting, Peak cladding temperature Corresponding boundary conditions during transients	
No. of Cases	Data supplied cases Exercise cases	4 2

Table 4.3.13 Test matrix of Transient Boiling Transition Measurements

Assembly	Initial Conditions				Transients	Exercise cases	No. of Cases
	Pressure (Mpa)	Power (MW)	Flow rate (t/h)	Inlet enthalpy (kJ/kg)			
C2A	7.2	6.2~8.5	45	1217~1227	Turbine trip without bypass	E	2
					Re-circulation pump trip	E	
C3	7.2	6.2~8.5	45	1217~1227	Turbine trip without bypass	-	2
					Re-circulation pump trip	-	

E: exercise case

Table 4.3.14 Test Numbers (No.) of Transient Boiling Transition Measurements

Test No.	Assembly	Initial Conditions				Transients	Exercise cases
		Pressure (Mpa)	Power (MW)	Flow rate (t/h)	Inlet enthalpy (kJ/kg)		
TGA10008	C2A	7.2	6.2~8.5	45	1217~1227	Turbine trip without bypass	E
TRA10012	C2A	7.2	6.2~8.5	45	1217~1227	Re-circulation pump trip	E
TGC10018	C3	7.2	6.2~8.5	45	1217~1227	Turbine trip without bypass	-
TIC10012	C3	7.2	6.2~8.5	45	1217~1227	Re-circulation pump trip	-

E: exercise case

Chapter 5

BECHMARK PHASES AND EXERCISES

5.1 Introduction

The OECD/NRC BFBT benchmark consists of two phases with each phase consisting of different exercises. The benchmark phases and exercises are described below.

Phase 1 – Void distribution benchmark

- Exercise 1 – Steady-state sub-channel grade benchmark
- Exercise 2 – Steady-state microscopic grade benchmark
- Exercise 3 – Transient macroscopic grade benchmark

Phase 2 – Critical power benchmark

- Exercise 1 – Steady-state benchmark
- Exercise 2 – Transient benchmark

The sub-channel approach is categorized as the macroscopic grade approach that can resolve an element as small as a sub-channel size mesh. Time and space averaged formulations cause the loss of the heterogeneous and instantaneous void fraction information of the two-phase flow structure within the sub-channel. As a consequence, many macroscopic correlations are still indispensable for reproducing the experimental results. In recent years, there have been developed newer two-phase flow numerical approaches that can be categorized into meso-, micro- or molecular dynamics approaches. For these situations, the void distributions within the sub-channel are calculated. Taking into account the immaturity of numerical modelling for detailed void distribution, this benchmark specification is designed to accept as many potential numerical approaches as possible.

The Table 5.1.1 provides a guide to the participants where to find the conditions for each benchmark case within each benchmark exercise and phase while the Table 5.1.2 provides a guide to the participants where to find the data for the involved fuel assemblies within these specifications.

Table 5.1.1 Benchmark Conditions

Benchmark phase	Exercises		Assembly ID	Geometrical data	Measurement conditions	Test matrix	Test numbers	Related section	Data format
Void distribution	**Steady state sub-channel**		0-1	Table 3.2.6	Table 5.2.1	Table 5.2.2	Table 5.2.3	Section 5.2.1	Table 5.2.4
			0-2	Table 3.2.6	Table 5.2.1	Table 5.2.2	Table 5.2.3	Section 5.2.1	Table 5.2.4
			0-3	Table 3.2.6	Table 5.2.1	Table 5.2.2	Table 5.2.3	Section 5.2.1	Table 5.2.4
			1	Table 3.2.7	Table 5.2.1	Table 5.2.2	Table 5.2.3	Section 5.2.1	Table 5.2.4
			2	Table 3.2.7	Table 5.2.1	Table 5.2.2	Table 5.2.3	Section 5.2.1	Table 5.2.4
			3	Table 3.2.7	Table 5.2.1	Table 5.2.2	Table 5.2.3	Section 5.2.1	Table 5.2.4
			4	Table 3.2.8	Table 5.2.1	Table 5.2.2	Table 5.2.3	Section 5.2.1	Table 5.2.4
	Steady state microscopic		0-1	Table 3.2.6	Table 5.2.1	Table 5.2.2	Table 5.2.3	Section 5.2.2	Table 5.2.5
			0-2	Table 3.2.6	Table 5.2.1	Table 5.2.2	Table 5.2.3	Section 5.2.2	Table 5.2.5
			0-3	Table 3.2.6	Table 5.2.1	Table 5.2.2	Table 5.2.3	Section 5.2.2	Table 5.2.5
			1	Table 3.2.7	Table 5.2.1	Table 5.2.2	Table 5.2.3	Section 5.2.2	Table 5.2.5
			2	Table 3.2.7	Table 5.2.1	Table 5.2.2	Table 5.2.3	Section 5.2.2	Table 5.2.5
			3	Table 3.2.7	Table 5.2.1	Table 5.2.2	Table 5.2.3	Section 5.2.2	Table 5.2.5
			4	Table 3.2.8	Table 5.2.1	Table 5.2.2	Table 5.2.3	Section 5.2.2	Table 5.2.5
	Transient macroscopic		4	Table 3.2.8	Table 5.2.3.1	Table 5.2.3.2	Table 5.2.3.3	Section 5.2.3	Table 5.2.3.4
Critical power	**Steady state**	*Pressure drop*	C2A {for single phase}	Table 3.2.8	Table 4.3.1	Table 4.3.2	Table 4.3.4	Section 4.3	-
			C2A {for two phase}	Table 3.2.8	Table 4.3.4	Table 4.3.5	Table 4.3.6	Section 4.3	
		Critical power	C2A	Table 3.2.8	Table 5.3.1.2	Table 5.3.1.3	Table 5.3.1.4	Section 5.3.1	Table 5.3.1.1
			C2B	Table 3.2.8	Table 5.3.1.2	Table 5.3.1.3	Table 5.3.1.4	Section 5.3.1	Table 5.3.1.1
			C3	Table 3.2.8	Table 5.3.1.2	Table 5.3.1.3	Table 5.3.1.4	Section 5.3.1	Table 5.3.1.1
	Transient		C2A	Table 3.2.8	Table 5.3.2.1	Table 5.3.2.2	Table 5.3.2.3	Section 5.3.2	Table 5.3.2.4
			C3	Table 3.2.8	Table 5.3.2.1	Table 5.3.2.2	Table 5.3.2.3	Section 5.3.2	Table 5.3.2.4

Table 5.1.2 Assembly Specification References

Assembly ID	Radial Power Shape	Axial power shape	Heater rod data	Spacer Type
0-1	uniform	Table 3.2.3	Table 3.3.1	Grid
0-2	uniform	Table 3.2.3	Table 3.3.1	Grid
0-3	uniform	Table 3.2.3	Table 3.3.1	Grid
1	Table 3.2.2	Table 3.2.3	Table 3.3.1	Grid
2	Table 3.2.2	Table 3.2.3	Table 3.3.1	Grid
3	Table 3.2.2	Table 3.2.3	Table 3.3.1	Grid
4	Table 3.2.5	Table 3.2.3	Table 3.3.1	Ferrule
C2A	Table 3.2.5	Table 3.2.3	Table 3.3.1	Ferrule
C2B	Table 3.2.5	Table 3.2.3	Table 3.3.1	Ferrule
C3	Table 3.2.5	Table 3.2.3	Table 3.3.1	Ferrule

5.2 Phase 1 - Void Distribution Benchmark

The steady state void distribution measured data is supplied as time-space averaged value in a sub-channel mesh size. However, the raw image data has a resolution as small as 0.3mm × 0.3mm and the liquid film on the rod surfaces can be roughly recognised from these images. This image data is recovered. It is transformed into the uncompressed ASCII image format and it is designed for benchmarking microscopic two-phase numerical approaches.

5.2.1 Exercise 1 – Steady State Sub-channel Grade Benchmark

The conditions for the steady state void distribution measurements are summarized in Table 5.2.1. The selected test cases for Exercise 1 are denoted with E1 in Tables 5.2.2 and 5.2.3. This exercise is designed for benchmarking sub-channel, meso- and microscopic numerical approaches. The supplied measured data includes time and space averaged void distribution matrix in sub-channel mesh size, and corresponding boundary conditions (pressure, flow, inlet sub-cooling, and power shape). Table 5.2.4 shows the data format of steady state sub- channel grade benchmark.

5.2.2 Exercise 2 – Steady State Microscopic Grade Benchmark

The selected test cases for Exercise 2 are denoted with E2 in Table 5.2.3. This exercise is designed for benchmarking meso-, micro-scopic, and molecular dynamics numerical approaches. The supplied measured data includes time and space averaged void distribution matrix with 0.3mm × 0.3mm mesh size and corresponding boundary conditions (pressure, flow, inlet sub-cooling, and power distribution). The Table 5.2.5 shows the data format of steady state microscopic grade benchmark.

Table 5.2.1 Steady-State Void Distribution Measurement Conditions

Assembly	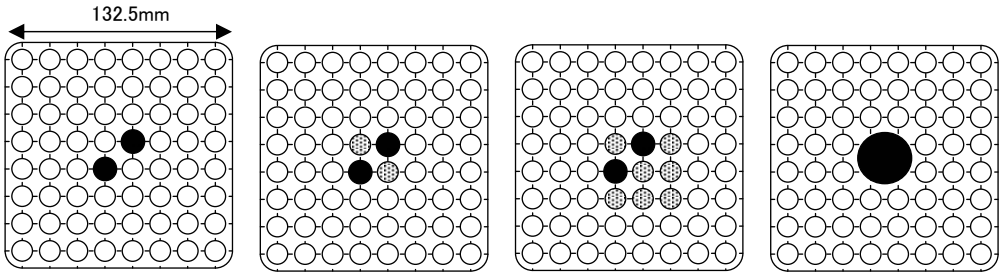	
Boundary Conditions	Pressure (MPa) Flow rate (t/h) Inlet sub-cooling (kJ/kg) Exit quality (%)	7.2 55 50.2 2 5 8 12 18 25
Data	Void distribution matrix in sub-channel mesh size Void distribution matrix in 0.3 × 0.3 mm mesh size (512 × 512 = 262K pixels) Corresponding boundary conditions	
No. of Cases	Exercise cases	sub-channel: 15 ; microscopic: 3

Exit quality: Thermal equilibrium quality

Table 5.2.2 Test Matrix of Steady-State Void Distribution Measurements

Assembly	Pressure (Mpa)	Inlet sub-cooling (kJ/kg)	Flow rate (t/h)	Exit quality (%)					
				2	5	8	12	18	25
0-1	7.2	50.2	55		E1		E1		E1
0-2	7.2	50.2	55		E1		E1		E1
0-3	7.2	50.2	55		E1		E1		E1
1	7.2	50.2	55		E1		E1		E1
4	7.2	50.2	55		E1,E2		E1,E2		E1,E2

E1: exercise 1 case, E2: exercise 2 case

Table 5.2.3 Test No. of Steady-State Void Distribution Measurements

Test No.	Assembly	Pressure (Mpa)	Flow rate (t/h)	Inlet sub-cooling (kJ/kg)	Exit quality (%)	Exercise cases	
0011-55	0-1	7.18	54.0	52.6	5.0	E1	-
0011-58	0-1	7.17	54.9	51.0	12.0	E1	-
0011-61	0-1	7.21	54.8	50.9	24.9	E1	-
0021-16	0-2	7.19	54.9	54.0	4.8	E1	-
0021-18	0-2	7.17	54.9	49.8	12.1	E1	-
0021-21	0-2	7.18	54.9	51.4	24.9	E1	-
0031-16	0-3	7.18	55.0	52.4	4.9	E1	-
0031-18	0-3	7.18	54.8	50.0	12.1	E1	-
0031-21	0-3	7.17	54.9	49.4	25.0	E1	-
1071-55	1	7.19	54.6	52.8	4.9	E1	-
1071-58	1	7.16	55.1	50.3	11.9	E1	-
1071-61	1	7.20	54.7	51.8	25.1	E1	-
4101-55	4	7.20	54.6	52.9	5.0	E1	E2
4101-58	4	7.15	54.6	50.6	12.1	E1	E2
4101-61	4	7.18	54.7	52.5	25.1	E1	E2

E1: case for exercise 1, E2: case for exercise 2

Table 5.2.4 Data Format of the Steady State Sub-channel Grade Void Distribution Benchmark

Test assembly type

System pressure= X.X MPa

Flow rate = X.X kg/m^2-s

Inlet sub-cooling= X.X °C

Power shape = -

	1	2	3	4	5	6	7	8
1	X.X	X.X	X.X	X.X	X.X	X.X	X.X	X.X
2	X.X	X.X	X.X	X.X	X.X	X.X	X.X	X.X
3	X.X	X.X	X.X	X.X	X.X	X.X	X.X	X.X
4	X.X	X.X	X.X	X.X	X.X	X.X	X.X	X.X
5	X.X	X.X	X.X	X.X	X.X	X.X	X.X	X.X
6	X.X	X.X	X.X	X.X	X.X	X.X	X.X	X.X
7	X.X	X.X	X.X	X.X	X.X	X.X	X.X	X.X
8	X.X	X.X	X.X	X.X	X.X	X.X	X.X	X.X

Table 5.2.5 Data Format of Steady State Microscopic Grade Void Distribution Benchmark

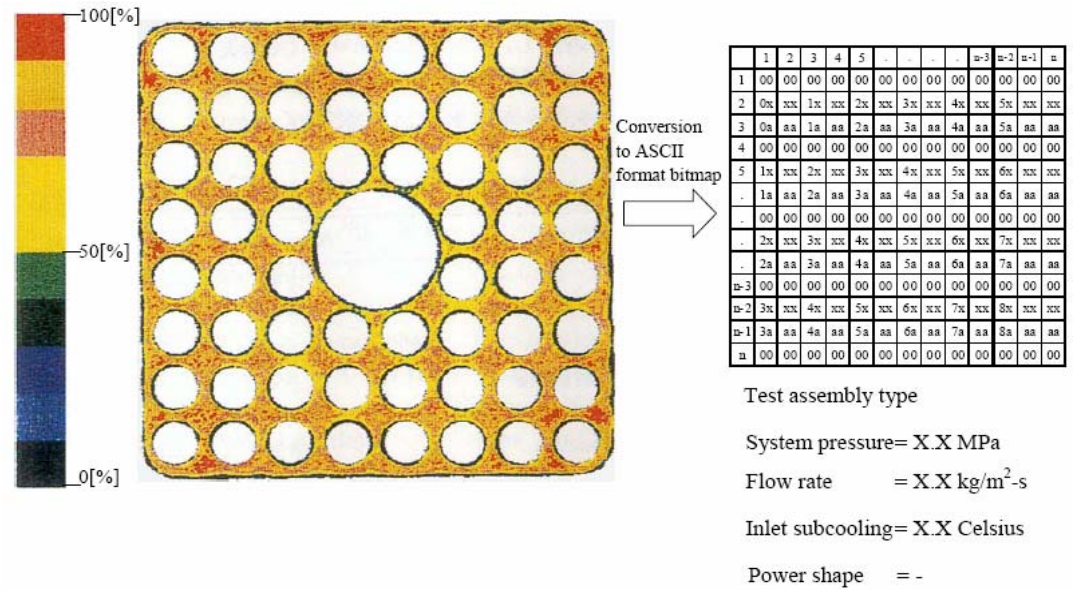

	1	2	3	4	5			.		n-3	n-2	n-1	n
1	00	00	00	00	00	00	00	00	00	00	00	00	00
2	0x	xx	1x	xx	2x	xx	3x	xx	4x	xx	5x	xx	xx
3	0a	aa	1a	aa	2a	aa	3a	aa	4a	aa	5a	aa	aa
4	00	00	00	00	00	00	00	00	00	00	00	00	00
5	1x	xx	2x	xx	3x	xx	4x	xx	5x	xx	6x	xx	xx
.	1a	aa	2a	aa	3a	aa	4a	aa	5a	aa	6a	aa	aa
.	00	00	00	00	00	00	00	00	00	00	00	00	00
.	2x	xx	3x	xx	4x	xx	5x	xx	6x	xx	7x	xx	xx
.	2a	aa	3a	aa	4a	aa	5a	aa	6a	aa	7a	aa	aa
n-3	00	00	00	00	00	00	00	00	00	00	00	00	00
n-2	3x	xx	4x	xx	5x	xx	6x	xx	7x	xx	8x	xx	xx
n-1	3a	aa	4a	aa	5a	aa	6a	aa	7a	aa	8a	aa	aa
n	00	00	00	00	00	00	00	00	00	00	00	00	00

5.2.3 Exercise 3 - Transient Macroscopic Grade Benchmark

The conditions for transient void distribution measurements are summarized in Table 5.2.3.1. In this exercise two transient cases, turbine trip without bypass and re-circulation pump trip, are selected. The selected test cases for the Exercise 3 are denoted with E3 in Tables 5.2.3.2 and 5.2.3.3. The Exercise 3 is designed for benchmarking sub-channel numerical approaches. The supplied measured data includes space averaged instantaneous axial void profiles during the transients and the corresponding boundary conditions (pressure, flow, inlet sub-cooling, and power shape). Table 5.2.3.4 shows the data format of transient sub channel grade benchmark.

Table 5.2.3.1 Transient Void Distribution Measurement Conditions

Assembly	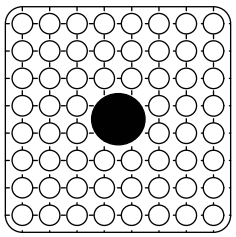 4	
Rated Initial Conditions	Pressure (MPa) Power (MW) Flow rate (t/h) Inlet temperature (Celsius)	7.2 4.5 55 279
Transients	Turbine trip without bypass, Re-circulation pump trip	
Data	Time histories of cross sectional averaged void fraction in each axial level during transients Corresponding boundary conditions during transients	
No. of Cases	Exercise cases	2

Table 5.2.3.2 Test Matrix of Transient Void Distribution Measurements

Assembly	Initial Conditions				Transients	Exercise cases
	Pressure (Mpa)	Power (MW)	Flow rate (t/h)	Inlet temperature (Celsius)		
4	7.2	4.5	55	279	Turbine trip without bypass	E3
					Re-circulation pump trip	E3

E3: case for exercise 3

Table 5.2.3.3 Test No. of Transient Void Distribution Measurements

Test No.	Assembly	Initial Conditions				Transients	Exercise cases
		Pressure (Mpa)	Power (MW)	Flow rate (t/h)	Inlet temperature (Celsius)		
4102-001~009	4	7.2	4.5	55	279	Turbine trip without bypass	E3
4102-019~027	4	7.2	4.5	55	279	Re-circulation pump trip	E3

E3: case for exercise 3

Table 5.2.3.4 Data Format of Transient Macroscopic Grade Void Distribution Benchmark

Cross-sectional averaged void fraction	Elevation-1	Elevation-2	….	Elevation-N-1	Elevation-N
Time1					
Time2					
Time3					
….					
TimeM-3					
TimeM-2					
TimeM-1					
TimeM					

Histories of boundary conditions	Pressure	Heat flux	Flow rate	Inlet temperature
Time1				
Time2				
Time3				
….				
TimeM-3				
TimeM-2				
TimeM-1				
TimeM				

Test assembly type
Power shape = -

5.3 Phase 2: Critical Power Benchmark

Basically, two approaches can be applied in the critical power benchmark:

1) One-dimensional approach with BT correlation. Participants may develop their own BT correlations based on test points. However, this will not be part of the objectives of this benchmark;

2) Sub-channel mechanistic approach.

5.3.1 Exercise 1 - Steady State Benchmark

The supplied measured data includes: single-phase pressure drop, two-phase pressure drop, critical power, axial location of boiling transition, and corresponding boundary conditions (pressure, flow, inlet sub-cooling, and power shape). The data format is given in Table 5.3.1.1. The test conditions are summarized in Tables 5.3.1.3 through 5.3.1.6. The selected test cases for Exercise 1 of Phase 2 are denoted with E1. The measured power is the bundle power at which dry out was detected.

Table 5.3.1.1 Data Format of Steady-State Critical Power Benchmark

No. of test points	Pressure	Flow rate	Inlet temperature	Pressure drop	Critical power	Location
1	Given	Given	Given	Measured	Measured	Measured
2	Given	Given	Given	Measured	Measured	Measured
3	Given	Given	Given	Measured	Measured	Measured
….						
151	Given	Given	Given	Measured	Measured	Measured

Test assembly type
Power shape = -

Table 5.3.1.2 Steady-State Critical Power Measurement Conditions

Assembly	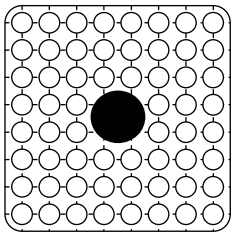 C2A 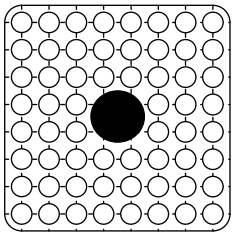 C2B 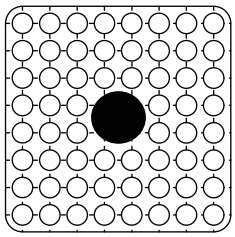 C3	
Boundary Conditions	Pressure (MPa) Flow rate (t/h) Inlet sub-cooling (kJ/kg)	5.5 7.2 8.6 10 20 30 45 55 60 65 25 50 84 104 126
Data	Critical power, Location of boiling transition Corresponding boundary conditions	
No. of Cases	Exercise cases	44

Table 5.3.1.3 Test Matrix of Steady-State Critical Power Measurements

Assembly	Pressure (Mpa)	Flow rate (t/h)	Inlet sub-cooling (kJ/kg)				
			25	50	84	104	126
C2A	5.5	20		E1			
		45		EX			
		55	E1	E1	E1		E1
		65		E1			
	7.2	20		E1			
		30		E1			
		45		E1			
		55	E1	E1	E1	E1	E1
		60		E1			
		65		E1			
	8.6	20		E1			
		45		E1			
		55	E1	E1	E1		E1
		65		E1			
C2B	7.2	20		E1			
		30		E1			
		45		E1			
		55	E1	E1	E1	E1	E1
		60		E1			
		65		E1			
C3	7.2	20		E1			
		30		E1			
		45		E1			
		55	E1	E1	E1	E1	E1
		60		E1			
		65		E1			

E1: exercise case

Table 5.3.1.4 Test No. of Steady-State Critical Power Measurements (C2A)

Test No.	Assembly	Pressure (Mpa)	Flow rate (t/h)	Inlet sub-cooling (kJ/kg)	Exercise cases
SA505500	C2A	5.49	20.16	50.95	E1
SA505501	C2A	5.49	20.10	51.35	E1
SA510500	C2A	5.48	55.06	56.41	E1
SA510501	C2A	5.51	55.11	62.48	E1
SA510600	C2A	5.51	54.70	96.16	E1
SA510601	C2A	5.52	55.34	96.79	E1
SA510800	C2A	5.51	54.81	134.97	E1
SA510900	C2A	5.52	54.70	35.33	E1
SA510901	C2A	5.51	55.05	35.02	E1
SA512500	C2A	5.54	65.48	64.36	E1
SA516500	C2A	5.51	44.85	55.98	E1
SA605500	C2A	7.16	20.09	50.55	E1
SA605502	C2A	7.17	20.07	51.44	E1
SA607500	C2A	7.13	30.02	48.35	E1
SA610503	C2A	7.17	55.20	59.39	E1
SA610504	C2A	7.17	55.47	58.09	E1
SA610600	C2A	7.18	55.05	89.53	E1
SA610700	C2A	7.13	55.20	107.61	E1
SA610701	C2A	7.21	54.88	113.28	E1
SA610800	C2A	7.24	55.30	137.26	E1
SA610900	C2A	7.27	55.10	37.73	E1
SA610902	C2A	7.18	55.42	32.94	E1
SA611500	C2A	7.13	60.23	54.89	E1
SA612500	C2A	7.16	65.36	55.66	E1
SA616500	C2A	7.13	45.17	54.21	E1
SA805500	C2A	8.63	20.30	51.00	E1
SA805501	C2A	8.64	20.30	50.28	E1
SA810501	C2A	8.62	55.15	54.89	E1
SA810502	C2A	8.64	55.16	55.12	E1
SA810600	C2A	8.56	55.00	83.85	E1
SA810601	C2A	8.64	55.21	88.54	E1
SA810800	C2A	8.64	55.28	130.30	E1
SA810900	C2A	8.66	55.38	30.97	E1
SA810901	C2A	8.60	55.15	27.55	E1
SA812500	C2A	8.64	65.25	58.08	E1
SA816500	C2A	8.61	45.24	52.22	E1

E1: exercise case

Table 5.3.1.5 Test No. of Steady-State Critical Power Measurements (C2B)

Run No.	Assembly	Pressure (Mpa)	Flow rate (t/h)	Inlet sub-cooling (kJ/kg)	Exercise cases
SB605500	C2B	7.15	20.03	51.66	E1
SB607500	C2B	7.13	30.05	49.90	E1
SB610500	C2B	7.2	54.84	54.28	E1
SB610501	C2B	7.19	54.91	51.16	E1
SB610600	C2B	7.18	54.91	82.45	E1
SB610700	C2B	7.18	54.71	105.31	E1
SB610800	C2B	7.14	54.90	122.48	E1
SB610900	C2B	7.2	54.88	26.55	E1
SB611500	C2B	7.19	59.88	54.03	E1
SB612500	C2B	7.18	64.60	48.65	E1
SB616501	C2B	7.14	44.82	47.96	E1

E1: exercise case

Table 5.3.1.6 Test No. of Steady-State Critical Power Measurements (C3)

Test No.	Assembly	Pressure (Mpa)	Flow rate (t/h)	Inlet sub-cooling (kJ/kg)	Exercise cases
SC605500	C3	7.16	19.96	50.40	E1
SC607500	C3	7.15	29.83	51.09	E1
SC616500	C3	7.15	45.04	50.88	E1
SC610900	C3	7.19	54.90	31.35	E1
SC610500	C3	7.19	54.90	50.74	E1
SC610502	C3	7.14	54.76	49.84	E1
SC610600	C3	7.13	54.66	81.93	E1
SC610700	C3	7.15	54.83	103.37	E1
SC610800	C3	7.21	55.06	128.69	E1
SC611500	C3	7.19	59.72	51.05	E1
SC612500	C3	7.17	65.02	52.32	E1

E1: exercise case

5.3.2 Exercise 2 - Transient Benchmark

The Exercise 2 of Phase 2 is designed for benchmarking one-dimensional approach with boiling transition correlation, and or a sub-channel mechanistic approach. The supplied measured data includes: timing of boiling transition, timing of rewetting, maximum rod surface temperature, location of boiling transition, histories of thermocouples, and corresponding boundary conditions (pressure, flow, inlet sub-cooling, and power shape). The data is provided in the format shown in Table 5.3.2.4. The test conditions are summarized in Tables 5.3.2.1 through 5.3.2.3. The selected cases for Exercise 2 of Phase 2 are denoted with E2.

Table 5.3.2.1 Transient Boiling Transition Measurement Conditions

Assembly	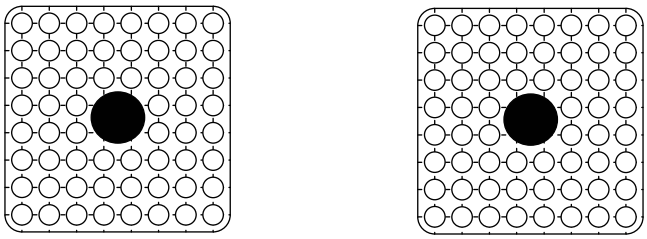	
Rated Initial Conditions	Pressure (MPa) Power (MW) Flow rate (t/h) Inlet enthalpy (kJ/kg)	7.2 6.2~8.5 45 1217~1227
Transients	Turbine trip without bypass Re-circulation pump trip	
Data	Time histories of cladding temperature where boiling transition occurred Timing of boiling transition, Timing of rewetting, Peak cladding temperature Corresponding boundary conditions during transients	
No. of Cases	Exercise cases	2

Table 5.3.2.2 Test Matrix of Transient Boiling Transition Measurements

Assembly	Initial Conditions				Transients	Exercise cases
	Pressure (Mpa)	Power (MW)	Flow rate (t/h)	Inlet enthalpy (kJ/kg)		
C2A	7.2	6.2~8.5	45	1217~1227	Turbine trip without bypass	E2
					Re-circulation pump trip	E2

E2: exercise case

Table 5.3.2.3 Test No. of Transient Boiling Transition Measurements

Test No.	Assembly	Initial Conditions				Transients	Exercise cases
		Pressure (Mpa)	Power (MW)	Flow rate (t/h)	Inlet enthalpy (kJ/kg)		
TGA10008	C2A	7.2	6.2~8.5	45	1217~1227	Turbine trip without bypass	E2
TRA10012	C2A	7.2	6.2~8.5	45	1217~1227	Re-circulation pump trip	E2

E2: exercise case

Table 5.3.2.4 Data Format of Transient Critical Power Benchmark

No. of test points	Transient type	Assembly type	Timing of BT	Maximum rod temp.	Timing of rewet
1	Given	–	Measured	Measured	Measured
2	Given	–	Measured	Measured	Measured
3	Given	–	Measured	Measured	Measured
…					

History of thermocouples	TC-1	TC -2	….	TC -N-1	TC –N
Time1					
Time2					
Time3					
….					
TimeM-3					
TimeM-2					
TimeM-1					
Time M					

Histories of boundary conditions	Pressure	Heat flux	Flow rate	Inlet temperature
Time1				
Time2				
Time3				
….				
TimeN-3				
TimeN-2				
TimeN-1				
Time N				

Chapter 6

OUTPUT REQUESTED

6.1 Introduction

The requested output information from the participants includes:

- Results should be presented on paper and electronic format (CD-ROM);
- All output should be in SI units;
- For time histories, output should be at 0.02 second intervals;
- Graphical comparison of calculated results and test data should be performed.

6.2 Void Distribution Benchmark

Exercise1: Steady-state sub-channel calculations

The calculated results, or output data, for a given exercise case should be submitted as a space averaged void distribution matrix in sub-channel mesh size. An example of the output format of the steady state sub-channel grade void distribution benchmark is given in Table 6.2.1.

Table 6.2.1 Output Format of Steady State Sub-Channel Grade Void Distribution Benchmark

Exercise 1, Phase 1
Test No.
Void Fraction, X.X %

	1	2	3	4	5	6	7	8	9
1	X.X	X.X	X.X	X.X	X.X	X.X	X.X	X.X	X.X
2	X.X	X.X	X.X	X.X	X.X	X.X	X.X	X.X	X.X
3	X.X	X.X	X.X	X.X	X.X	X.X	X.X	X.X	X.X
4	X.X	X.X	X.X	X.X	X.X	X.X	X.X	X.X	X.X
5	X.X	X.X	X.X	X.X	X.X	X.X	X.X	X.X	X.X
6	X.X	X.X	X.X	X.X	X.X	X.X	X.X	X.X	X.X
7	X.X	X.X	X.X	X.X	X.X	X.X	X.X	X.X	X.X
8	X.X	X.X	X.X	X.X	X.X	X.X	X.X	X.X	X.X
9	X.X	X.X	X.X	X.X	X.X	X.X	X.X	X.X	X.X

Cross-sectional averaged: %

Exercise 2: Steady-state microscopic calculations

Output data should be a void distribution matrix in 0.3 mm × 0.3 mm mesh size. The data format of the steady state microscopic grade void distribution benchmark is given in Table 6.2.2.

Table 6.2.2 Output Format of Steady State Microscopic Grade Void Distribution Benchmark

Exercise 2, Phase 1
Test No.
Void Fraction, X.X %

	1	2	3	.	.	.	.	n-1	n
1	X.X	X.X	X.X	X.X	X.X	X.X	X.X	X.X	X.X
2	X.X	X.X	X.X	X.X	X.X	X.X	X.X	X.X	X.X
3	X.X	X.X	X.X	X.X	X.X	X.X	X.X	X.X	X.X
.	X.X	X.X	X.X	X.X	X.X	X.X	X.X	X.X	X.X
.	X.X	X.X	X.X	X.X	X.X	X.X	X.X	X.X	X.X
.	X.X	X.X	X.X	X.X	X.X	X.X	X.X	X.X	X.X
.	X.X	X.X	X.X	X.X	X.X	X.X	X.X	X.X	X.X
n-1	X.X	X.X	X.X	X.X	X.X	X.X	X.X	X.X	X.X
n	X.X	X.X	X.X	X.X	X.X	X.X	X.X	X.X	X.X

Cross-sectional averaged: %

Exercise 3: Transient macroscopic calculations

Output data should be space averaged instantaneous axial void profiles at the specified times during the transient. This data should be for the turbine trip without bypass and the re-circulation pump trip transients.

Output format for this exercise is summarized in Table 6.2.3.

Table 6.2.3 Output format of Transient Macroscopic Grade Void Distribution Benchmark

Exercise 3, Phase 1
Test No.
Void Fraction, X.X %

Cross-sectional averaged void fraction	Elevation-1	Elevation-2	….	Elevation-N-1	Elevation-N
Time1					
Time2					
Time3					
….					
TimeM-3					
TimeM-2					
TimeM-1					
TimeM					

6.3. Critical Power Benchmark

Exercise 1: Steady state critical power benchmark calculations

The requested output is the pressure drop profile along the heated length at critical power and the critical power location of boiling transition and critical power value.

The required output for the steady-state benchmark includes:

- Pressure drop distribution profile along the heated length at critical power;
- Critical power, value, location;
- Axial location of boiling transition;
- Quality/void profile at critical power;
- Rod surface temperature profile at critical power.

For the three-field sub-channel codes, the additional outputs will be:

- Detailed radial location of boiling transition;
- Liquid film thickness profile at critical power;
- Droplet entrainment fraction profile at critical power.

The data format for this exercise is summarized in Table 6.3.1.

Table 6.3.1 Output Format of Steady State Critical Power Benchmark

Test No.	Pressure drop	Critical power	Axial location

Exercise 2: Transient critical power benchmark calculations

The requested output data is the timing of boiling transition, timing of rewetting, maximum rod surface temperature, and location of boiling transition and histories of thermocouples. The data format for this exercise summarized in Table 6.3.2.

Table 6.3.2 Output Format of Transient Critical Power Benchmark

Test No.	Location of BT	Maximum rod temp.	Timing of rewet	Timing of BT

REFERENCES

[1] R. T. Lahey, and F. J. Moody, "The Thermal Hydraulics of a Boiling Water Nuclear Reactor." American Nuclear Society (ANS), 1977

[2] R. T. Lahey, et al., "Two-phase flow and Heat Transfer in Multi-rod Geometries: Sub-channel and Pressure Drop Measurements in Nine-Rod Bundle for Diabatic and Adiabatic Conditions", GEAP-13049 AEC Research and Development Report, March 1970

[3] H. Herkenrath, et al.: Experimental Investigation of the Enthalpy and Mass Flow Distribution in 16-Rod Cluster with BWR, PWR – Geometries and Conditions. Final Report. EUR 7575 EN, Joint Research Center Ispra, Italy, 1981.

[4] Summary of the 4th OECD/NRC BWR TT Workshop, October 4, 2002, Seoul, Korea.

[5] A. Inoue, T. Kurosu, T. Aoki, and M. Yagi, "Void Fraction Distribution in BWR Fuel Assembly and Evaluation of Sub-channel Code", Journal of Nuclear science and Technology, July,1995

[6] H. Utsuno, N. Ishida, Y. Masuhara, and F. Kasahara, "Assessment of Boiling Transition Analysis Code Against Data from NUPEC BWR Full-size Fine-mesh Bundle Tests", Proceedings of NUTHOS-6 Conference, Nara, Japan, October 8, 2004.

[7] E. Sartori, L.. Hochreiter, K. Ivanov, and H. Utsuno, "The OECD/NRC BWR Full-size Fine-Mesh Bundle Tests Benchmark (BFBT) - General Description", Proceedings of NUTHOS-6 Conference, Nara, Japan, October 8, 2004.

[8] "TRAC-PF1/MOD2 Theory Manual, Appendix B, Material Properties", NUREG/CR-5673 (1993).